Chemical catalyst manipulating cancer epigenome and transcription

Yuki Yamanashi[1], Shinpei Takamaru[1], Atsushi Okabe[2, 3], Satoshi Kaito[4], Yuto Azumaya[1], Yugo R. Kamimura[1], Kenzo Yamatsugu[1], Tomoya Kujirai[5], Hitoshi Kurumizaka[5], Atsushi Iwama[4], Atsushi Kaneda[2, 3], Shigehiro A. Kawashima[1]*, Motomu Kanai[1]*

[1]Graduate School of Pharmaceutical Sciences, The University of Tokyo; Bunkyo-ku, Tokyo, 113-0033, Japan, [2]Molecular Oncology, Graduate School of Medicine, Chiba University; Chuo-ku, Chiba, 260-8670, Japan, [3]Health and Disease Omics Center, Chiba University; Chuo-ku, Chiba, 260-8670, Japan [4]Division of Stem Cell and Molecular Medicine, Center for Stem Cell Biology and Regenerative Medicine, The Institute of Medical Science, The University of Tokyo; Minato-ku, Tokyo, 108-8639, Japan, [5]Institute for Quantitative Biosciences, The University of Tokyo; Bunkyo-ku, Tokyo, 113-0032, Japan

Corresponding Authors:
Motomu Kanai
kanai@mol.f.u-tokyo.ac.jp

Shigehiro A. Kawashima
skawashima@mol.f.u-tokyo.ac.jp

1

Abstract

Post-translational modification (PTM) of histones dynamically regulates gene transcription and is closely related to cancer development. Altering the epigenome is thus a promising strategy for cancer chemotherapy. However, there have been no methods to artificially introduce physiologically relevant histone PTMs and their transcription profile without genetic engineering in living cells. Here we report a cell-permeable histone acetylation catalyst, BAHA-LANA-PEG-CPP44, enabling cancer epigenome manipulation. The catalyst selectively entered leukemia cells, bound to chromatin, and selectively acetylated H2BK120 of endogenous histones in a short reaction time. The catalytic histone acetylation attenuated chromatin binding of negative elongation factor E (NELFE), an RNA polymerase II regulatory factor, and changed the transcription profile in leukemia cells. The in-cell chemical catalysis slowed proliferation of leukemia cells and reduced their tumorigenic potential in mice. As this approach requires no genetic engineering and is orthogonal to canonical epigenetic drugs, it may represent a new modality of cancer chemotherapy.

2

In eukaryotic cells, genomic DNA wraps around a histone octamer, consisting of two copies of each of the four core histones (H2A, H2B, H3, and H4), to form a nucleosome, the fundamental unit of chromatin. Post-translational modifications (PTMs) of histones, such as phosphorylation, ubiquitination, methylation, and acetylation, in nucleosomes make up a large part of the epigenome and have a fundamental role in determining chromatin structure and function. Euchromatin (open chromatin) is generally marked by histone acetylation and related to active transcription and gene expression, while heterochromatin (closed chromatin) is generally marked by histone methylation and suppresses transcription. The level of histone PTM is tightly regulated by chromatin-modifying enzymes (writers and erasers) in living organisms. In the case of histone acetylation, histone acetyltransferases (HATs) catalyze the addition of an acetyl group to a histone lysine residue, while histone deacetylases (HDACs) remove the acetylation.

An abnormal epigenome and abnormal gene expression are hallmarks of cancer[1, 2, 3, 4]. Thus, methods that can manipulate the epigenome in cancer hold promise for therapeutic applications. Small molecule inhibitors of chromatin-modifying enzymes, such as HDAC inhibitors, have been developed as anti-cancer drugs and approved by the FDA[5, 6, 7, 8]. However, this approach might be ineffective when the target enzymes acquire genetic mutations affecting enzyme activity or drug efficacy. The direct promotion of histone PTMs in living cells by an artificial means, bypassing endogenous chromatin-modifying enzymes, is an emerging, alternative strategy. These methods include genetic code expansion[9, 16], split intein ligation[17, 18], dCas9-writer/eraser fusion proteins[11, 19], and chemical catalysis[20, 21, 22]. Among them, the chemical catalysis approach, in which chemical catalysts directly promote histone PTMs without relying on chromatin-modifying enzymes, does not require genetic engineering, and thus could substantially benefit biology and medicine.

Our group previously reported a histone acetylation catalyst, PEG-LANA-DSSMe, in which a prodrug disulfide form of a thiol-tethered 4-dimethylaminopyridine (DSH) catalyst is conjugated with a histone-binding LANA (latency associated nuclear antigen) peptide and a poly(ethylene glycol) (PEG) moiety[20]. The PEG-LANA-DSH catalyst binds to the acidic patch of nucleosomes via LANA, and efficiently promotes histone- and regio-selective acetylation of the proximal H2BK120 residue in living cells, using thioester acetyl donors. However, a high

3

concentration of acetyl donor (30 mM) was necessary for efficient histone acetylation, due to its moderate catalyst activity. Furthermore, since PEG-LANA-DSSMe was cell-impermeable, this approach relied on a bead-loading method to introduce the catalysts into living cells and thus had limited utility, especially for therapeutic purposes. In this study, we developed novel cell-permeable chemical catalysts that promote physiologically relevant histone acetylation without relying on HAT enzymes in tumor cells and proposed the concept of "catalytic epigenome therapy", in which the cancer epigenome can be manipulated by chemical catalysts.

Development of a cell-permeable histone acylation catalyst targeting H2BK120

Synthetic H2BK120 acylation was expected to modulate the transcription profile by attenuating inter-nucleosomal interaction[23] or inhibiting H2B ubiquitination[20]. Therefore, we sought to design new chemical catalysts that could selectively acylate H2BK120 by crossing the cell membrane, migrating to the nucleus, binding to the H2BK120-proximal acidic patch on the nucleosome, and activating a stable acyl donor molecule (Fig. 1a). We envisioned a chemical catalyst comprised of four motifs that could achieve catalytic histone acylation in living cells (Fig. 1a): a cell-penetrating peptide (CPP) to permeate the cell membrane, a LANA peptide to bind the nucleosome acidic patch, PEG to shield LANA from peptidases, and a catalytically active site (CAS) to activate an acyl donor for lysine acylation.

We began our study from the catalyst structure optimization at the CAS motif. There are two CAS candidates functional in living cells; DSH, which activates thioesters, such as acyl-CoAs, through dynamic thiol-thioester exchange and intramolecular acyl group transfer to form a reactive acyl pyridinium intermediate [23], and boronate-assisted hydroxamic acid (BAHA), which is composed of a hydroxamic acid moiety and a diol moiety[24] (for the chemical structures and reaction mechanisms of CASs, see Extended Data Fig. 1). BAHA recruits boronic acid-containing acyl donors to the diol moiety and generates reactive acyl hydroxamate intermediates through the subsequent intramolecular acyl group transfer. We compared these CASs and found that BAHA showed higher histone acetylation activity than DSH, especially under BSO (an inhibitor of glutathione synthesis)-free conditions (Extended Data Fig. 2a-c), suggesting that BAHA is more resistant to intracellular glutathione than DSH. Next, we optimized LANA

4

and PEG motifs. Previous study suggested that conjugation of a PEG motif to the C-terminus of LANA decreased the affinity of LANA with nucleosomes[20]. Therefore, we screened the PEG-conjugation position by substituting each amino acid of the LANA$_{5-15}$ peptide to an acetylated lysine, used as a model for PEG-conjugated lysine, and found that the 13th serine was the best position for PEG conjugation (Extended Data Fig. 3a-d). Finally, we optimized the CPP motif. We first conjugated oligo-arginine peptides[25, 26, 27], such as 8r and 16r (an 8-mer and a 16-mer of D-arginine, respectively), to FITC-labeled LANA-PEG compounds and examined their membrane permeability for HeLa S3 cells (cervical cancer cell line). When FITC-LANA-PEG-8r (**S22**, Extended Data Fig. 4a, 50 µM) was added to cell culture media, fluorescent signals mainly localized in endosomes, suggesting that **S22** failed to escape from endosomes (Extended Data Fig. 4b). For FITC-LANA-PEG-16r (**S27**, Extended Data Fig. 4c), 16r was conjugated with FITC-LANA-PEG via a disulfide bond, with the expectation that the disulfide bond would be cleaved by glutathione to release FITC-LANA-PEG in the cells. While **S27** localized in nuclei at 5 µM (Extended Data Fig. 4d), no nuclear localization was observed at 2 µM (Extended Data Fig. 4d). We also confirmed chromatin localization of **S27** (5 µM) in HEK293T cells (embryonic kidney cell line) (Extended Data Fig. 4e). Taken together, **S27** permeated through cell membranes and localized at chromatin in both HeLa S3 and HEK293T cells. We then conjugated cell type-selective CPPs, such as leukemia cell-selective CPP44[28]. FITC-LANA-PEG-CPP44 (**S34**, Extended Data Fig. 5a), but not FITC-LANA-PEG (**S32**, Extended Data Fig. 5a), efficiently entered THP-1 cells (MLL-rearrangement leukemia cell line) and localized at chromatin, while **S34** did not enter HeLa S3 cells or PBMC (peripheral blood mononuclear cells) (Fig. 2a, b). **S34** failed to enter THP-1 cells when a dynamin inhibitor was added or at 4 °C (Extended Data Fig. 5b, c), suggesting that the cell penetrating mechanism of **S34** into THP-1 cells was through a dynamin- and ATP-dependent endocytic pathway, as suggested by the previous report[28]. Based on these optimizations, we synthesized BAHA-LANA-PEG-CPP44 (**1**: Fig. 1b) as a leukemia cell-selective catalyst, and BAHA-LANA-PEG-16r (**S30**: Extended Data Fig. 4c), which may have no cell-type selectivity, as a catalyst for non-leukemia cells.

In-cell H2BK120 acetylation by cell-permeable histone acylation catalysts
We examined the cytotoxicity of BAHA-LANA-PEG-16r catalyst (**S30**) in HeLa S3 cells. While 2 µM **S30** did not show apparent cytotoxicity, greater than 5 µM **S30**

5

was cytotoxic (Extended Data Fig. 4f). We then evaluated the effects of the CPP motif by comparing the in-cell histone acetylation activity of **S30** and CPP-non-conjugated BAHA-LANA-PEG catalyst (**3**) using HeLa S3 and HEK293T cells. After cells were treated with **S30** or **3** (5 µM) and acetyl donor **4** (0.4 mM), the cells were stained with 4′,6-diamidine-2-phenylindole dihydrochloride (DAPI) to exclude potential artifacts caused by contaminated dead cells. We sorted DAPI-negative cells (i.e., living cells) and examined acetylation of H2BK120 by both immunoblot analysis using a H2BK120ac-specific antibody and LC-MS/MS analysis. Remarkably, **S30**, but not **3**, promoted H2BK120 acetylation in both HeLa S3 and HEK293T cells (Extended Data Fig. 4g, h). However, acetylation stoichiometry was low (~ 5% yield) (Extended Data Fig. 4i), which limited utility of **S30**.

Next, we examined the cytotoxicity of BAHA-LANA-PEG-CPP44 catalyst (**1**) and found that less than 20 µM **1** did not show any cytotoxicity in THP-1 cells (Fig. 2c). We also confirmed that less than 2 mM acetyl donor **4** was not toxic in THP-1 cells (Fig. 2d). As a negative control catalyst, we synthesized BAHA-mutLANA-PEG-CPP44 (**2**), lacking nucleosome-binding ability (Fig. 1b, Extended Data Fig. 5d). We confirmed that **1** and **3**, but not **2**, had histone acetylation ability for recombinant nucleosomes in test tubes (Fig. 3e). We then assessed in-cell histone acetylation activity. We added 10 µM **1** and 1 mM **4** to the culture media of THP-1 cells and examined acetylation of H2BK120 by immunoblot. H2BK120 acetylation was significantly promoted by **1** and **4** combined, but not by **1** or **4** alone (Fig. 3f). H2BK120 ubiquitination was reduced by catalytic H2BK120 acetylation promoted by **1** and **4**, as was observed previously (Fig. 3f)[20]. **2** or **3** with **4** did not promote H2BK120 acetylation in THP-1 cells, confirming that both LANA and CPP44 were essential for in-cell histone acetylation activity of the catalyst (Fig. 3f).

Characterization of the catalytic histone acetylation in leukemia cells

Since the catalytic histone acetylation by **1** inhibited Mg^{2+}-promoted nucleosome self-association and the formation of phase-separated 12-mer nucleosome arrays *in vitro* (Extended Data Fig. 6a-c), we expected that H2BK120 acetylation may attenuate inter-nucleosomal interaction and affect chromatin structures as well as gene transcription in cells. Therefore, we characterized the catalytic histone acetylation by **1** in THP-1 cells in detail.

Catalyst **1** with acetyl donor **4** promoted histone-selective acetylation, and other

6

proteins showed little to no acetylation (Extended Data Fig. 7a). To evaluate lysine residue selectivity, we quantified the acetylation stoichiometry of histone's lysine residues by LC-MS/MS analysis. The result showed that the main acetylation site was H2BK120 (~38% yield, Fig. 2g). H2BK116 and H2AK15 were slightly acetylated (~5% yield), and other lysine residues, including those in H3 or H4 tail, were rarely acetylated (Fig. 2g). Catalyst **1** promoted acetylation of H2BK120 when H2BK120ac writer enzymes p300 (KAT3B) and CBP (KAT3A)[29] were knocked down with RNAi (Extended Data Fig. 7b). Furthermore, treatment of THP-1 cells with an HDAC inhibitor SAHA did not affect catalyst-dependent H2BK120 acetylation (Extended Data Fig. 7c). These results indicate that H2BK120ac was directly introduced by catalyst **1** and the acetylation reaction did not depend on cellular HAT or HDAC activity.

The BAHA catalyst promotes not only acetylation but also other acylations, including non-natural ones, simply by changing acyl donors[24]. Therefore, we prepared acyl donors with pentynoyl **S35**, azidobutyryl **S36**, methyl succinyl **S37**, and butyryl **S38** groups (Extended Data Fig. 8a) and conducted in-cell acylation reactions with catalyst **1**. As expected, the addition of **1** and the acyl donors to THP-1 cells promoted histone acylation in all cases (Extended Data Fig. 8b-c). We showed that catalytically incorporated azidobutyrylated histones can be labeled by alkyne-conjugated TAMRA via click chemistry, visualizing endogenous histones in THP-1 cells (Extended Data Fig. 8d).

To address the cell-type selectivity of the catalytic histone acetylation reaction, we treated various leukemia cell lines (THP-1, MOLM-13, MV-4-11, Kasumi-1, and K562) and non-leukemia cell lines (HeLa S3, HEK293T, and PBMC) with 10 µM **1** and 1 mM **4** and examined acetylation of H2BK120 by immunoblot analysis (Fig. 3h). Consequently, H2BK120 acetylation was promoted by **1** with **4**, but not by **2** with **4**, in all the leukemia cell lines, while it was hardly promoted in non-leukemia cell lines (Fig. 3h). These data showcased the high leukemia cell-selectivity of the catalytic histone acetylation.

Transcriptional changes and anti-leukemia effects induced by catalytic histone acetylation

To investigate whether the catalytic histone acetylation affected the transcription profile, we performed transcriptome analysis. RNA sequencing (RNA-seq) of acetylated THP-1 cells treated with **1** and **4** for 4 hours identified 634 upregulated (UP) and 466 downregulated (DOWN) genes compared to unacetylated THP-1

7

cells treated with **2** and **4** for 4 hours (Fig. 3a). Since the catalytic histone acetylation reduced ubiquitination of H2B (Fig. 2f), which is required for the expression of MLL-fusion target genes in MLL-rearranged leukemia cells[30], we first assessed transcriptional changes of 330 MLL-fusion target genes. However, transcription of MLL-fusion target genes was largely unchanged by the catalytic histone acetylation (Fig. 3b), probably due to insufficient reduction of H2B ubiquitination. We then conducted Gene Ontology (GO) analysis to identify that UP genes were related to regulation of apoptosis, cell cycle, or transcription (Extended Data Fig. 9a), although DOWN genes did not have such significant features (Extended Data Fig. 9b). We further confirmed this correlation by RT-qPCR analysis of selected genes related to these GO-terms, such as EGR1, JUN, or p21 (Extended Data Fig. 10a). Consistently, the catalytic histone acetylation induced cell cycle arrest at G1/S phase and apoptosis in THP-1 cells (Fig. 3c, d). Next, we investigated whether catalytic histone acetylation affects proliferation of leukemia cells. When histones in THP-1 cells were acetylated by **1** and **4**, the proliferation of THP-1 cells was inhibited for several days (Fig. 3e). In contrast, the treatment with **2** and **4** did not inhibit proliferation (Fig. 3e), indicating that the proliferation inhibition was the consequence of the catalytic histone acetylation. The anti-proliferative effects of catalytic histone acetylation were not only observed in the MLL-rearrangement leukemia cells (THP-1, MOLM-13, MV-4-11), but also leukemia cells without MLL translocations (Kasumi-1, K562) (Fig. 3f). In contrast, the proliferation of HeLa S3 cells was not affected by the treatment with **1** and **4** (Fig. 3f), confirming the leukemia cell-selectivity of the catalyst. We also tested the *in vivo*-tumorigenic potential of the catalytic histone acetylation in leukemia cells. The Akaluc-bearing MOLM-13 leukemia cells were acetylated by **1** and **4**, and then intravenously injected to NOG mice. As a result, the mice treated with acetylated MOLM-13 cells showed significantly slower cancer progression and longer survival than the mice treated with unacetylated MOLM-13 cells using **2** and **4** (Fig. 3f, g). These results demonstrate that the catalytic histone acetylation reduced the tumorigenic potential of leukemia cells both *in vitro* and *in vivo*.

Mechanistic insight into transcriptional changes by catalytic histone acetylation

To explore how the catalytic histone acetylation affects gene transcription, more specifically how upregulated genes are differentiated from other genes, we

8

studied the transcriptional changes immediately following the reaction. The time-course analysis of the reaction progress in THP-1 cells showed that H2BK120 acetylation proceeded within 30 min of the treatment with **1** and **4**, and reached a plateau at approximately 60 min (Fig. 4a). This kinetic profile was similar to that of histone-tail acetylation after treatment with an HDAC inhibitor, SAHA (Fig. 4a). Thus, we analyzed transcriptional changes at 45 min after the treatment with catalyst **1** or **2** and acetyl donor **4**. RNA-seq of acetylated THP-1 cells with **1** and **4** identified 124 upregulated (UP) and 105 downregulated (DOWN) genes compared to unacetylated THP-1 cells treated with **2** and **4** (Fig. 4b). We examined chromatin binding of RNA polymerase II (Pol II) after the catalytic histone acetylation by chromatin immunoprecipitation sequencing (ChIP-seq) and found that chromatin binding of RNA Pol II was significantly increased in UP genes (Fig. 4c, d). This result suggests that the catalytic histone acetylation promoted transcription of subset of genes by RNA Pol II.

We initially hypothesized that the observed transcriptional changes induced by the catalytic histone acetylation were due to the difference in the H2BK120 acetylation level depending on the gene locus. Thus, we conducted ChIP-seq analyses of H2BK120ac. However, the H2BK120 acetylation level increased both in UP and DOWN genes (Fig. 4d, e). Because catalyst **1** consistently bound to nucleosomes irrespective of the gene loci, H2BK120 acetylation was not gene-selective. Thus, we alternatively assumed that a specific transcription factor (TF) was involved in the selective transcriptional changes. We searched for TFs correlated with UP or DOWN genes in the Encyclopedia of DNA Elements (ENCODE) Transcription Factor Targets dataset to identify that UP genes, but not DOWN genes, significantly correlated to the binding sites of negative elongation factor E (NELFE) in human leukemia cell line K562 (Fig. 4f, Extended Data Fig. 9c). NELFE is a component of a negative elongation factor (NELF) complex. ChIP-seq analyses of NELFE in unacetylated THP-1 cells treated with **2** and **4** confirmed the localization of NELFE in significantly higher levels at UP genes than others (Fig. 4g). We then examined if the catalytic histone acetylation with **1** and **4** affects chromatin binding of NELFE. ChIP-seq analyses of NELFE in THP-1 cells showed that the chromatin localization of NELFE was notably reduced by the catalytic histone acetylation (Fig. 5e, h), while the protein level of NELFE in the whole cell was comparable between acetylated and unacetylated cells (Fig. 5i). The catalytic histone acetylation comprehensively reduced the localization of NELFE in gene loci with high and low levels of NELFE (Extended Data Fig. 10b).

https://doi.org/10.26434/chemrxiv-2024-g1cq3 **ORCID:** https://orcid.org/0000-0002-2946-6627 Content not peer-reviewed by ChemRxiv. **License:** CC BY-NC-ND 4.0

Interestingly, transcription of genes with high-level NELFE was significantly enhanced by the catalytic histone acetylation, whereas transcription of genes with low-level NELFE was not affected (Fig. 5j). This result suggests that high-level NELF inhibits gene transcription, while the catalytic histone acetylation induces the release of NELF from chromatin and mitigates the inhibitory effects of high-level NELF (Fig. 5k). Overall, the observed gene selectivity in transcriptional upregulation by the catalytic histone acetylation is likely due to the distribution of high-level NELF on chromatin.

Discussion

Although previous reports showed chromatin localization of H2BK120ac on transcriptionally active genes[29, 31], functions of H2BK120ac have remained unclear. BAHA-LANA-PEG-CPP44 catalyst **1** selectively acetylated H2BK120 in living cells and thus can be used to address the downstream consequences of H2BK120ac. The fact that chromatin localization of NELFE was reduced immediately after H2BK120 acetylation suggests the role of H2BK120ac to release NELF complex from chromatin in THP-1 leukemia cells. Further analysis is needed to elucidate the mechanisms of releasing NELF by H2BK120 acetylation. A reader protein of H2BK120ac might be involved in this process, but such a protein has not been identified yet. NELF was initially isolated from human nuclear extract as a complex that prevents RNA Pol II-dependent transcription on a naked DNA template[32]. Although *in-vitro* biochemical and structural studies indicated the role of NELF in RNA pol II pausing at the promoter-proximal region[33, 34, 35], the function of NELF in cells is yet to be fully elucidated. While NELF is essential for regulation of promoter-proximal RNA Pol II in the *hsp70* gene in *Drosophila*[36, 37], several *in-vivo* studies showed that not all promoter-proximal pausing is dependent on NELF[38, 39, 40]. Furthermore, a recent study suggested that NELF plays a positive role in transcription elongation by stabilizing 5' end of transcripts[38]. Our data showed that transcription of genes with high-level NELFE was upregulated by the catalytic histone acetylation, which likely supports the negative role of NELF in transcriptional elongation. However, the fact that the catalytic histone acetylation also downregulated transcription of a subset of genes may reflect the positive roles of NELF in transcriptional elongation.

Several reports showed that knockout or knockdown of NELF inhibited the development of various cancers[41, 42, 43, 44], suggesting that NELF acts as an oncoprotein and is a potential target of cancer chemotherapy. Our observations

that the catalytic histone acetylation furnished anti-leukemia effects are likely due to loss of chromatin localization of NELF. Catalyst **1** acetylates H2BK120, but not lysine residues in histone tails, the main targets of endogenous HAT and HDAC enzymes. Therefore, the catalytic histone acetylation is orthogonal to cancer epigenetic drugs targeting histone-modifying enzymes, such as HDAC inhibitors. The anti-cancer effects of our catalyst approach would be further enhanced by combining with HDAC inhibitors. This is the first example of intervening cancer epigenome and changing the transcription profile in living cells entirely relying on the chemical catalysis independent of enzymatic processes. The BAHA-LANA-PEG-CPP44 catalyst **1**-acyl donor **4** system is highly modulable (Fig. 1b). For example, changing CPP44 to other CPPs, such as CPP2[28], may realize catalytic histone acetylation in cancer cells other than leukemia cells as CPP determines the cell-selectivity. Changing the position of the catalytically active BAHA motif on the LANA ligand may change the regioselectivity of histone acetylation, since the BAHA catalyst selectively acetylated a proximal lysine. Changing the acyl group of **4** switches the acyl group introduced to H2BK120 and likely modulates the anti-cancer effects. Furthermore, other PTMs, such as lysine methylation or tyrosine phosphorylation, can be incorporated into histones when BAHA is changed to an alternate catalytically active motif promoting the intended PTM, which is under development in our group. We envision that the "catalytic epigenome therapy" presented here will lead to a new modality of anti-cancer therapy in the future.

11

References

1. Timp W, Feinberg AP. Cancer as a dysregulated epigenome allowing cellular growth advantage at the expense of the host. *Nat Rev Cancer* 2013, **13**(7)**:** 497-510.

2. Audia JE, Campbell RM. Histone Modifications and Cancer. *Csh Perspect Biol* 2016, **8**(4).

3. Flavahan WA, Gaskell E, Bernstein BE. Epigenetic plasticity and the hallmarks of cancer. *Science* 2017, **357**(6348).

4. Costa PMD, Sales SLA, Pinheiro DP, Pontes LQ, Maranhao SS, Pessoa CD*, et al.* Epigenetic reprogramming in cancer: From diagnosis to treatment. *Front Cell Dev Biol* 2023, **11**.

5. Johnstone RW. Histone-deacetylase inhibitors: Novel drugs for the treatment of cancer. *Nat Rev Drug Discov* 2002, **1**(4)**:** 287-299.

6. Szyf M. Epigenetics, DNA Methylation and Chromatin Modifying Drugs. *Annu Rev Pharmacol* 2009, **49:** 243-263.

7. Eckschlager T, Plch J, Stiborova M, Hrabeta J. Histone Deacetylase Inhibitors as Anticancer Drugs. *Int J Mol Sci* 2017, **18**(7).

8. Mohammad HP, Barbash O, Creasy CL. Targeting epigenetic modifications in cancer therapy: erasing the roadmap to cancer. *Nat Med* 2019, **25**(3)**:** 403-418.

9. de la Torre D, Chin JW. Reprogramming the genetic code. *Nat Rev Genet* 2021, **22**(3)**:** 169-184.

10. Muller MM, Muir TW. Histones: At the Crossroads of Peptide and Protein Chemistry. *Chem Rev* 2015, **115**(6)**:** 2296-2349.

11. Nakamura M, Gao Y, Dominguez AA, Qi LS. CRISPR technologies for precise epigenome editing. *Nat Cell Biol* 2021, **23**(1)**:** 11-22.

12. Yamatsugu K, Kawashima SA, Kanai M. Leading approaches in synthetic epigenetics for novel therapeutic strategies. *Curr Opin Chem Biol* 2018, **46:** 10-17.

13. Yamaguchi Y, Shibata H, Handa H. Transcription elongation factors DSIF and NELF: Promoter-proximal pausing and beyond. *Bba-Gene Regul Mech* 2013, **1829**(1)**:** 98-104.

14. Schier AC, Taatjes DJ. Structure and mechanism of the RNA polymerase II transcription machinery. *Gene Dev* 2020, **34**(7-8)**:** 465-488.

15. Aoi Y, Shilatifard A. Review Transcriptional elongation control in developmental gene expression, aging, and disease. *Mol Cell* 2023, **83**(22)**:** 3972-3999.

16. Elsässer SJ, Ernst RJ, Walker OS, Chin JW. Genetic code expansion in stable cell lines enables encoded chromatin modification. *Nat Methods* 2016, **13**(2)**:** 158-+.

17. David Y, Vila-Perelló M, Verma S, Muir TW. Chemical tagging and customizing of cellular chromatin states using ultrafast
-splicing inteins. *Nat Chem* 2015, **7**(5)**:** 394-402.

18. Burton AJ, Haugbro M, Parisi E, Muir TW. Live-cell protein engineering with an ultra-short split intein. *Proc Natl Acad Sci U S A* 2020, **117**(22)**:** 12041-12049.

19. Thakore PI, Black JB, Hilton IB, Gersbach CA. Editing the epigenome: technologies for programmable transcription and epigenetic modulation. *Nat Methods* 2016, **13**(2)**:** 127-137.

20. Fujiwara Y, Yamanashi Y, Fujimura A, Sato Y, Kujirai T, Kurumizaka H*, et al.* Live-cell epigenome manipulation by synthetic histone acetylation catalyst system. *Proc Natl Acad Sci U S A* 2021, **118**(4).

13

21. Fujimura A, Ishida H, Nozaki T, Terada S, Azumaya Y, Ishiguro T*, et al.* Designer Adaptor Proteins for Functional Conversion of Peptides to Small-Molecule Ligands toward In-Cell Catalytic Protein Modification. *ACS Cent Sci* 2023, **9**(11)**:** 2115-2128.

22. Habazaki M, Mizumoto S, Kajino H, Kujirai T, Kurumizaka H, Kawashima SA*, et al.* A chemical catalyst enabling histone acylation with endogenous acyl-CoA. *Nat Commun* 2023, **14**(1)**:** 5790.

23. Amamoto Y, Aoi Y, Nagashima N, Suto H, Yoshidome D, Arimura Y*, et al.* Synthetic Posttranslational Modifications: Chemical Catalyst-Driven Regioselective Histone Acylation of Native Chromatin. *J Am Chem Soc* 2017, **139**(22)**:** 7568-7576.

24. Adamson C, Kajino H, Kawashima SA, Yamatsugu K, Kanai M. Live-Cell Protein Modification by Boronate-Assisted Hydroxamic Acid Catalysis. *J Am Chem Soc* 2021, **143**(37)**:** 14976-14980.

25. Futaki S, Suzuki T, Ohashi W, Yagami T, Tanaka S, Ueda K*, et al.* Arginine-rich peptides - An abundant source of membrane-permeable peptides having potential as carriers for intracellular protein delivery. *J Biol Chem* 2001, **276**(8)**:** 5836-5840.

26. Allen JK, Brock DJ, Kondow-McConaghy HM, Pellois JP. Efficient Delivery of Macromolecules into Human Cells by Improving the Endosomal Escape Activity of Cell-Penetrating Peptides: Lessons Learned from dfTAT and its Analogs. *Biomolecules* 2018, **8**(3).

27. Patel SG, Sayers EJ, He L, Narayan R, Williams TL, Mills EM*, et al.* Cell-penetrating peptide sequence and modification dependent uptake and subcellular distribution of green florescent protein in different cell lines. *Sci Rep-Uk* 2019, **9**.

28. Kondo E, Saito K, Tashiro Y, Kamide K, Uno S, Furuya T*, et al.* Tumour lineage-homing cell-penetrating peptides as anticancer molecular delivery systems. *Nat Commun* 2012, **3**.

14

29.   Gatta R, Dolfini D, Zambelli F, Imbriano C, Pavesi G, Mantovani R. An acetylation-mono-ubiquitination switch on lysine 120 of H2B. *Epigenetics-Us* 2011, **6**(5)**:** 630-637.

30.   Wang E, Kawaoka S, Yu M, Shi JW, Ni T, Yang WJ*, et al.* Histone H2B ubiquitin ligase RNF20 is required for MLL-rearranged leukemia. *P Natl Acad Sci USA* 2013, **110**(10)**:** 3901-3906.

31.   Wang ZB, Zang CZ, Rosenfeld JA, Schones DE, Barski A, Cuddapah S*, et al.* Combinatorial patterns of histone acetylations and methylations in the human genome. *Nat Genet* 2008, **40**(7)**:** 897-903.

32.   Yamaguchi Y, Takagi T, Wada T, Yano K, Furuya A, Sugimoto S*, et al.* NELF, a multisubunit complex containing RD, cooperates with DSIF to repress RNA polymerase II elongation. *Cell* 1999, **97**(1)**:** 41-51.

33.   Vos SM, Farnung L, Urlaub H, Cramer P. Structure of paused transcription complex Pol II-DSIF-NELF. *Nature* 2018, **560**(7720)**:** 601-+.

34.   Renner DB, Yamaguchi Y, Wada T, Handa H, Price DH. A highly purified RNA polymerase II elongation control system. *J Biol Chem* 2001, **276**(45)**:** 42601-42609.

35.   Yamaguchi Y, Inukai N, Narita T, Wada T, Handa H. Evidence that negative elongation factor represses transcription elongation through binding to a DRB sensitivity-inducing factor/RNA polymerase II complex and RNA. *Mol Cell Biol* 2002, **22**(9)**:** 2918-2927.

36.   Wu CH, Yamaguchi Y, Benjamin LR, Horvat-Gordon M, Washinsky J, Enerly E*, et al.* NELF and DSIF cause promoter proximal pausing on the hsp70 promoter in Drosophila. *Gene Dev* 2003, **17**(11)**:** 1402-1414.

37.   Wu CH, Lee C, Fan RP, Smith MJ, Yamaguchi Y, Handa H*, et al.* Molecular characterization of NELF. *Nucleic Acids Res* 2005, **33**(4)**:** 1269-1279.

38. Aoi Y, Smith ER, Shah AP, Rendleman EJ, Marshall SA, Woodfin AR*, et al.* NELF Regulates a Promoter-Proximal Step Distinct from RNA Pol II Pause-Release. *Mol Cell* 2020, **78**(2)**:** 261-+.

39. Booth GT, Wang IX, Cheung VG, Lis JT. Divergence of a conserved elongation factor and transcription regulation in budding and fission yeast. *Genome Res* 2016, **26**(6)**:** 799-811.

40. Fant CB, Levandowski CB, Gupta K, Maas ZL, Moir J, Rubin JD*, et al.* TFIID Enables RNA Polymerase II Promoter-Proximal Pausing. *Mol Cell* 2020, **78**(4)**:** 785-+.

41. Zhang JQ, Hu ZH, Chung HH, Tian Y, Lau KW, Ser Z*, et al.* Dependency of NELF-E-SLUG-KAT2B epigenetic axis in breast cancer carcinogenesis. *Nat Commun* 2023, **14**(1).

42. Ghouraba MH, Masad RJ, Mpingirika EZ, Abdelraheem OM, Zeghlache R, Alserw AM*, et al.* Role of NELF-B in supporting epithelial-mesenchymal transition and cell proliferation during hepatocellular carcinoma progression. *Oncol Lett* 2021, **22**(5).

43. El Zeneini E, Kamel S, El-Meteini M, Amleh A. Knockdown of COBRA1 decreases the proliferation and migration of hepatocellular carcinoma cells. *Oncol Rep* 2017, **37**(3)**:** 1896-1906.

44. Aoki K, Nitta A, Igarashi A. NELF and PAF1C complexes are core transcriptional machineries controlling colon cancer stemness. *Oncogene* 2024.

46 Stasevich, T. J. *et al.* Regulation of RNA polymerase II activation by histone acetylation in single living cells. *Nature* **516**, 272–275 (2014).

47. Ishiguro, T. *et al.* Synthetic Chromatin Acylation by an Artificial Catalyst System. *Chem* **2**, 840–859 (2017).

48. Kayamori, K. *et al.* DHODH inhibition synergizes with DNA-demethylating agents in the treatment of myelodysplastic syndromes. *Blood Adv.* **5**, 438–450 (2021).

17

Figures
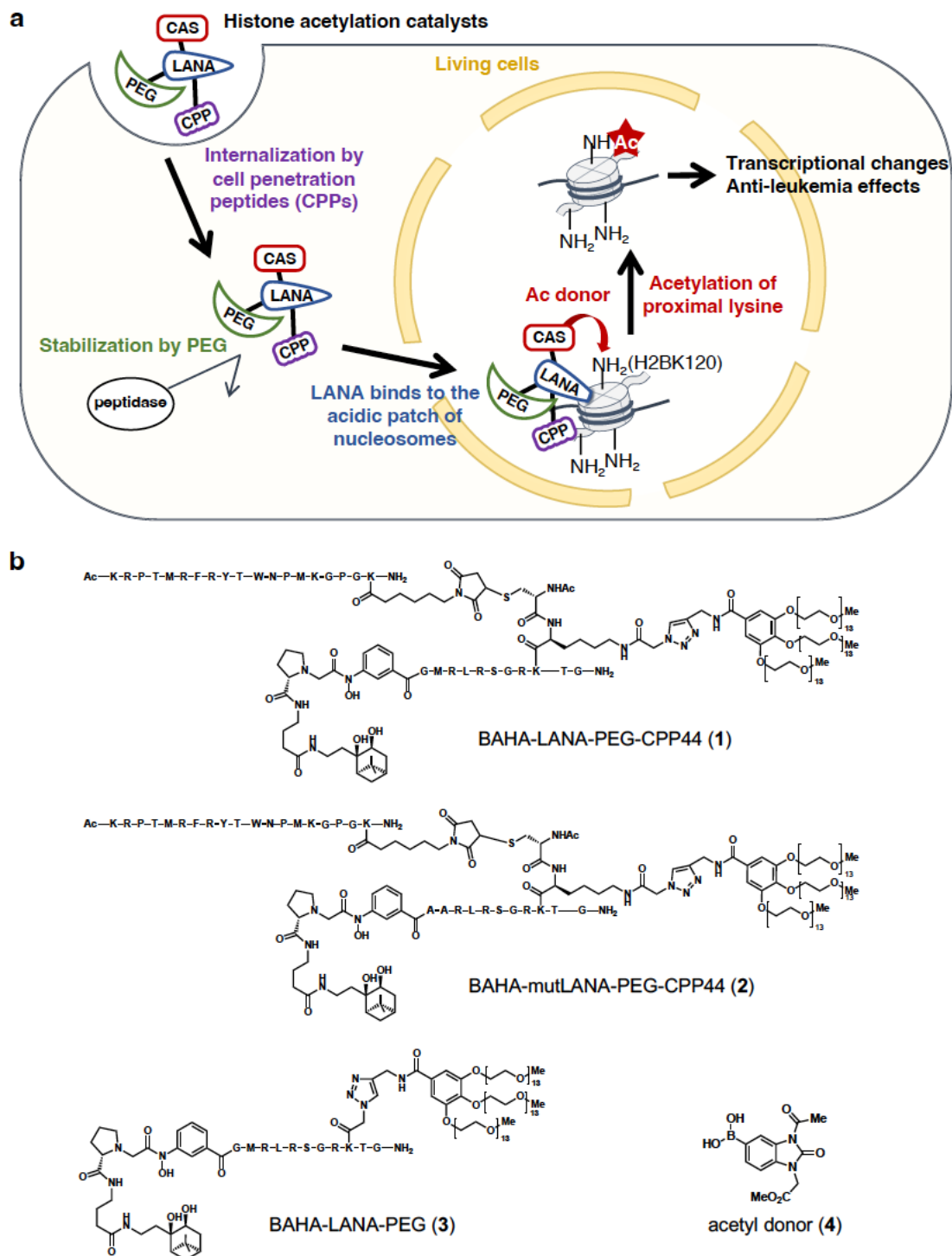
Fig. 1: Schematics of catalytic histone acetylation in living cells and chemical structures of catalysts and acetyl donor used in this study.

a, The BAHA-LANA-PEG-CPP44 catalyst penetrates the cell membrane via a cell penetrating peptide (CPP). Poly(ethylene glycol) (PEG) shields the LANA

peptide from peptidases. The LANA peptide binds the acidic patch of nucleosomes, and a catalytically active site (CAS) promotes the acetylation of a proximal lysine residue in histones using an acetyl donor. **b,** Structures of BAHA-LANA-PEG-CPP44 **1**, BAHA-mutLANA-PEG-CPP44 **2**, BAHA-LANA-PEG **3**, and acetyl donor **4**.
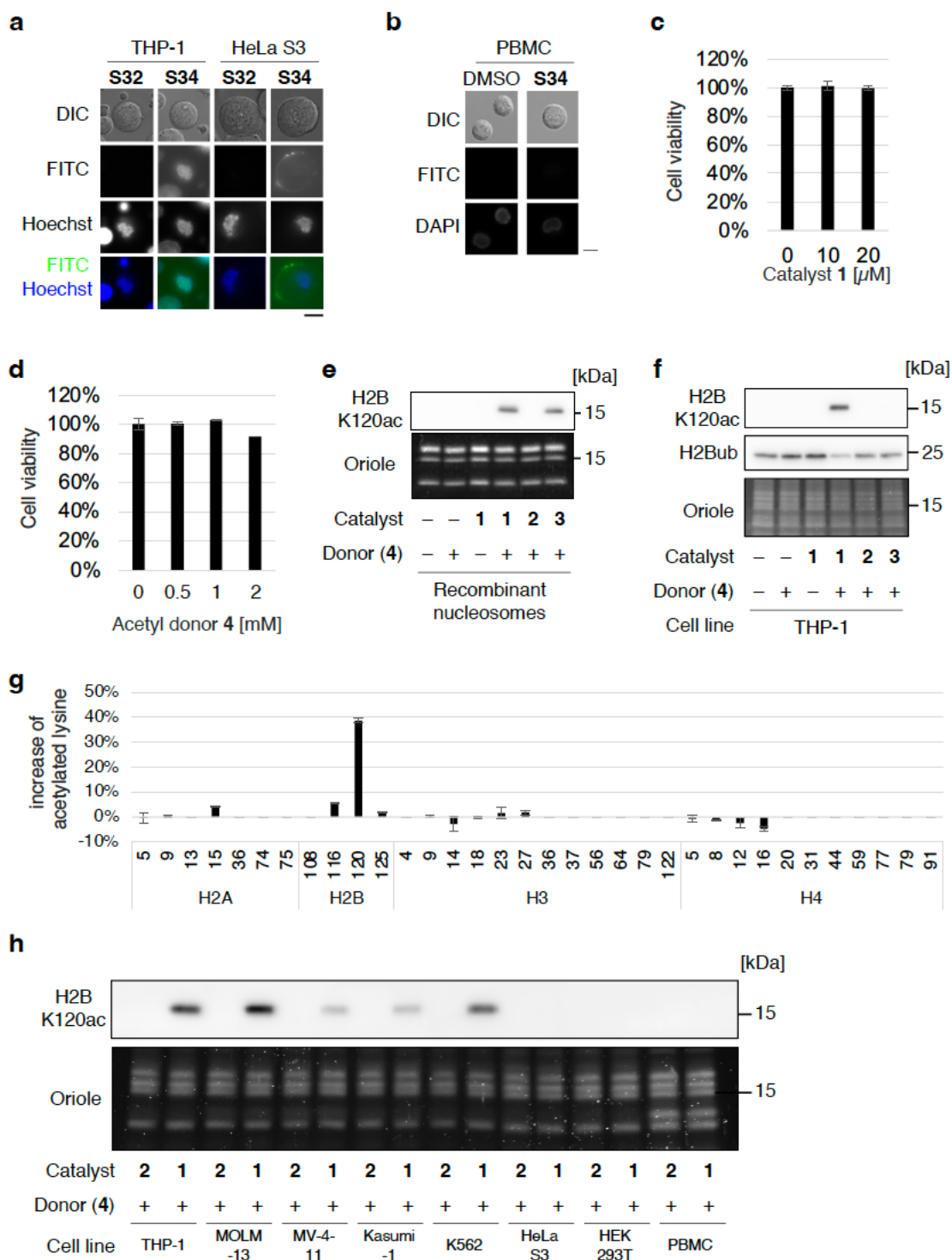
Fig. 2: BAHA-LANA-PEG-CPP44 catalyst promoted H2BK120 acetylation in leukemia cells.

a-b, Cells were treated with **S32** or **S34** (50 µM) for 60 min. Representative microscopic images of FITC-LANA$_{S13K}$-PEG$_{550}$ **S32** and FITC-LANA$_{S13K}$-PEG$_{550}$-CPP44 **S34** in the indicated cell line. DNA was stained with Hoechst 33342 to

20

visualize chromatin distribution. Scale bar, 10 μm. **c-d**, Cytotoxicity of catalyst **1** or acetyl donor **4**. THP-1 cells were treated with **1** or **4** for 6 hours. Error bars represent the data range of two independent experiments. **e,** Immunoblot showing H2BK120 acetylation (H2BK120ac) levels of recombinant nucleosomes treated with catalyst **1**, **2**, or **3** (2 μM) and acetyl donor **4** (0.1 mM) for 2 hours. **f,** Immunoblot showing H2BK120ac and H2BK120 ubiquitination (H2Bub) levels in THP-1 cells treated with catalyst **1**, **2**, or **3** (10 μM) and acetyl donor **4** (1 mM) for 4 hours. **g**, LC-MS/MS analysis for lysine acetylation levels of histone H2A, H2B, H3, or H4 in THP-1 cells treated with catalyst **1** or **2** (10 μM) and acetyl donor **4** (1 mM) for 4 hours. The acetylation yield was calculated as the ratio of acetylated lysine to (acetylated lysine + unmodified lysine) detected by LC-MS/MS, and the difference of the yield with **1** from the yield with **2** is shown. Each number corresponds to the position of lysine residue in the histone protein. **h**, Immunoblot showing H2BK120ac levels in the indicated cell lines treated with catalyst **1** or **2** (10 μM) and acetyl donor **4** (1 mM) for 2 hours. The loading amounts of histones were visualized with Oriole staining in **e-g**.
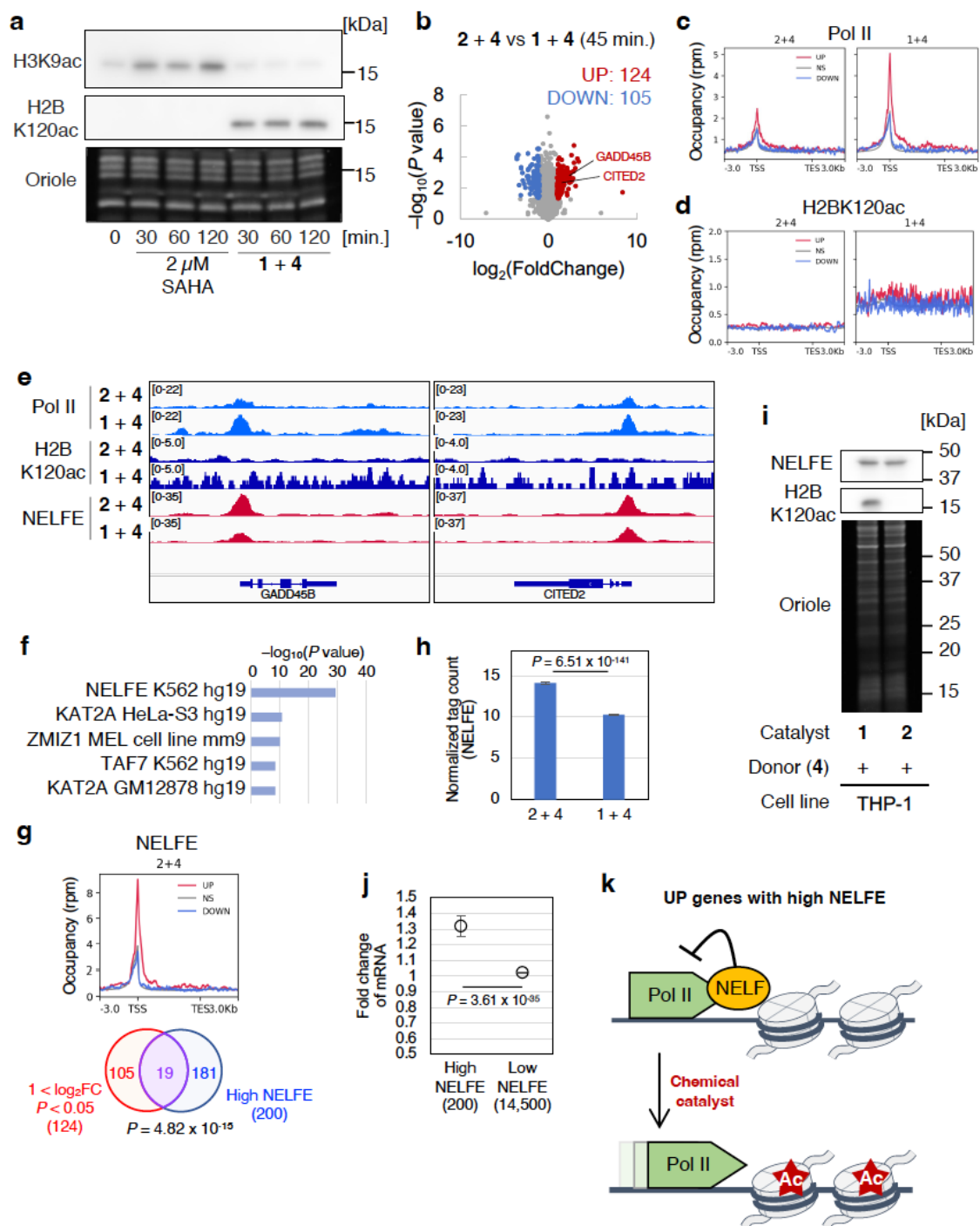
21
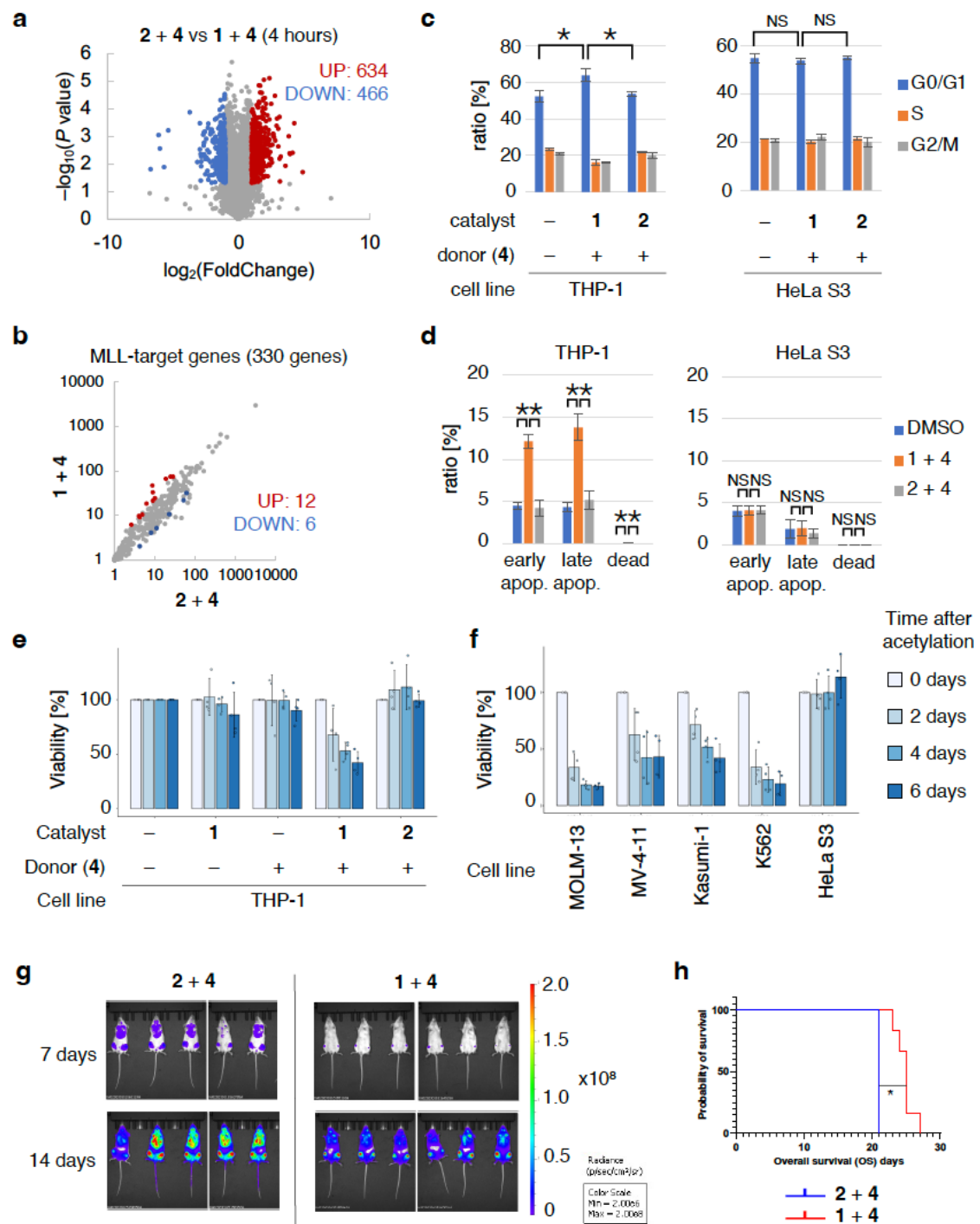
Fig. 3: Transcriptional changes and anti-leukemia effects induced by catalytic histone acetylation.

Before analysis, cells were treated with catalyst **1** or **2** (10 μM) and acetyl donor **4** (1 mM) for 4 hours. **a-b**, Correlation between catalytic histone acetylation and gene transcription. After acetylation for 4 hours, THP-1 cells were analyzed by

RNA-seq. In **a** and **b**, red and blue dots represent significantly upregulated and downregulated genes, respectively ($P < 0.05$, $\log_2$FC > 1 or < 1). Gray dots represent other genes (NS). **a,** Volcano plot denoting differential expression of genes. **b**, Scatter plot of the FPKM+1 value of MLL-fusion target genes (Human Gene Set: KUMAR_TARGETS_OF_MLL_AF9_FUSION). **c,** Correlation between catalyst-promoted acetylation and cell cycles. Cells were treated with catalyst **1** or **2** (10 μM) and acetyl donor **4** (1 mM) for 4 hours, and the medium was replaced with fresh medium. After 18 h, cells with different cell cycle (G0/G1, S, or G2/M) were classified by flow cytometry for DNA content. Error bars represent the standard deviation of three independent experiments (*$P < 0.05$, one-way ANOVA with Tukey's post hoc test, NS: not significant). **d**, Correlation between catalyst-promoted acetylation and apoptosis. Cells were treated with catalyst **1** or **2** (10 μM) and acetyl donor **4** (1 mM) for 4 hours, and the medium was replaced with fresh medium. After 48 hours, cells with early apoptosis (apop.), late apoptosis, or dead were classified by flow cytometry for Annexin V and 7-AAD staining. Error bars represent the standard deviation of three independent experiments (*$P < 0.05$, one-way ANOVA with Tukey's post hoc test, NS: not significant). **e-f**, Correlation between catalytic histone acetylation and proliferation of cell lines. After acetylation for 4 hours, the medium was replaced with fresh medium. The numbers of trypan blue-negative cells at 0-6 days are shown, normalized to DMSO-treated cells in **e** or **4**-treated cells in **f**. Error bars represent the standard deviation of four independent experiments. **g-h**, Correlation between catalytic histone acetylation and the tumorigenic potential in mice. After acetylation for 4 hours, Akaluc-expressing 3×10^6 MOLM-13 cells were intravenously injected to NOG mice. **g**, Images of bioluminescence signals in recipient mice at 7 and 14 days post-transplantation. **h**, A Kaplan-Meier survival. Statistical significance was calculated in comparison of **1**+**4** to **2**+**4** treated cells with log-rank tests. *$P < 0.05$.

Fig. 4: Mechanistic insights into transcriptional changes by catalytic histone acetylation.

Before analysis, THP-1 cells were treated with catalyst **1** or **2** (10 µM) and acetyl donor **4** (1 mM) for 0-120 min in **a**, or 45 min in **b-j**. **a**, Immunoblot showing histone modification levels after catalytic histone acetylation (**1+4**) or SAHA (2 µM) treatment. **b**, Volcano plot denoting differential expression of genes in RNA-seq

analysis was shown. Red and blue dots represent significantly upregulated (UP) and downregulated (DOWN) genes, respectively ($P < 0.05$, $\log_2$FC > 1 or < 1). Gray dots represent other genes (NS). **c-d**, Metagene profiles in ChIP-seq analyses of RNA polymerase II (Pol II) in **c** or H2BK120ac in **d** were shown. Red and blue lines represent significantly upregulated (UP) and downregulated (DOWN) genes in **b**, respectively ($P < 0.05$, $\log_2$FC > 1 or < 1). Gray lines represent other genes (NS). **e**, Genome browser track example of the ChIP-seq data over the GADD45B and CITED2 loci visualized by the Integrated Genomics Viewer (IGV). **f**, Top-5 enriched clusters of ENCODE TF ChIP-seq 2015 library from enrichment analysis of upregulated genes ($\log_2$FC > 1). **g**, Metagene profiles in ChIP-seq analyses of NELFE were shown. Venn diagram indicating overlapping upregulated (UP) genes and high NELFE genes, which had top-200 normalized tag count of NELFE ChIP-seq. The *P*-value was calculated by Fisher's exact test. **h**, Comparison of the change of normalized tag count of NELFE ChIP-seq after acetylation. Data are shown as mean ± SEM (n = 13,710). The *P*-value was calculated by Student's *t*-test. **i**, Immunoblot showing NELFE and H2BK120ac after catalytic histone acetylation. The loading amounts of proteins were visualized with Oriole staining. **j**, Comparison of the fold change of mRNA levels after catalytic histone acetylation. Data are shown as mean ± SEM (n = 200 for high NELFE genes, 14,500 for low NELFE genes). The *P*-value was calculated by Student's *t*-test. **k**, A plausible mechanism of transcriptional activation of UP genes with high NELFE by the catalytic histone acetylation. See Discussion section for details.
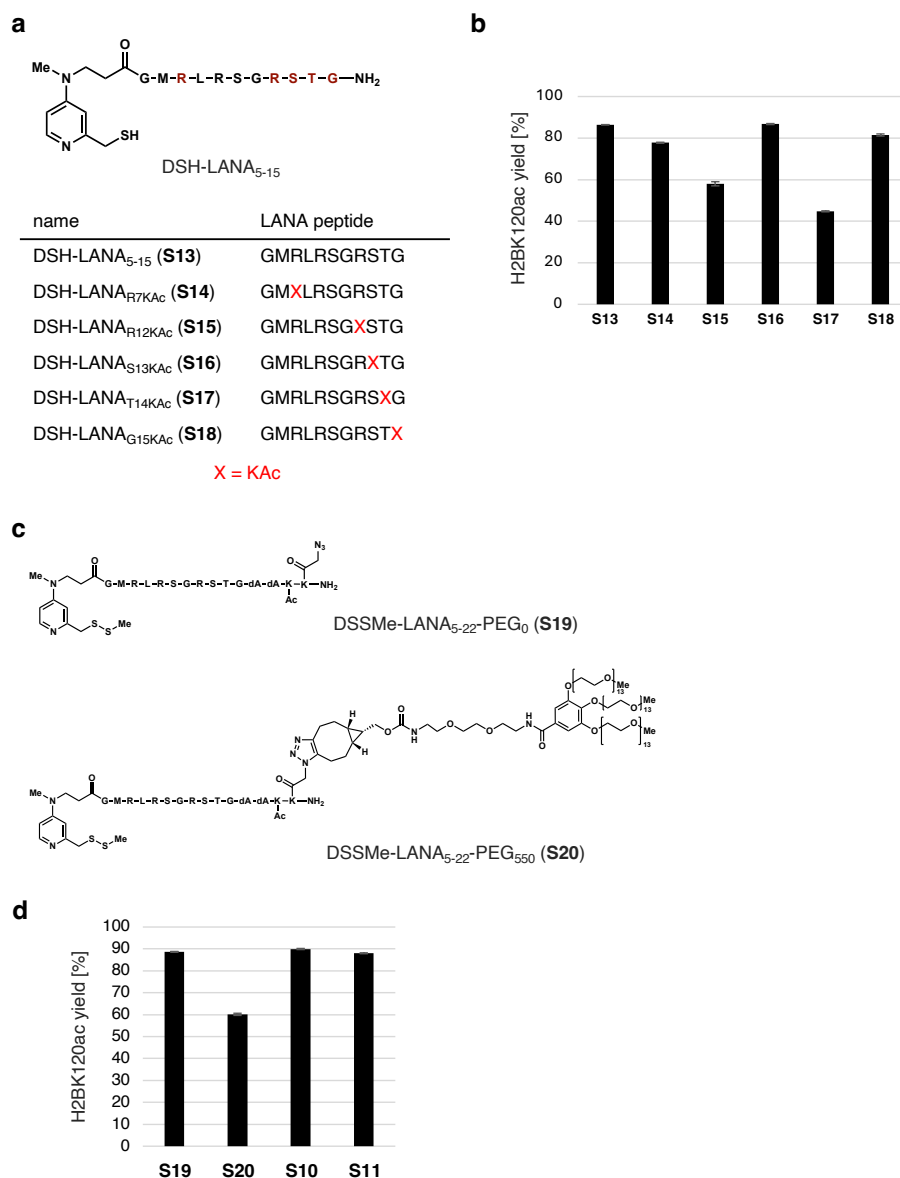
Extended Data Figures
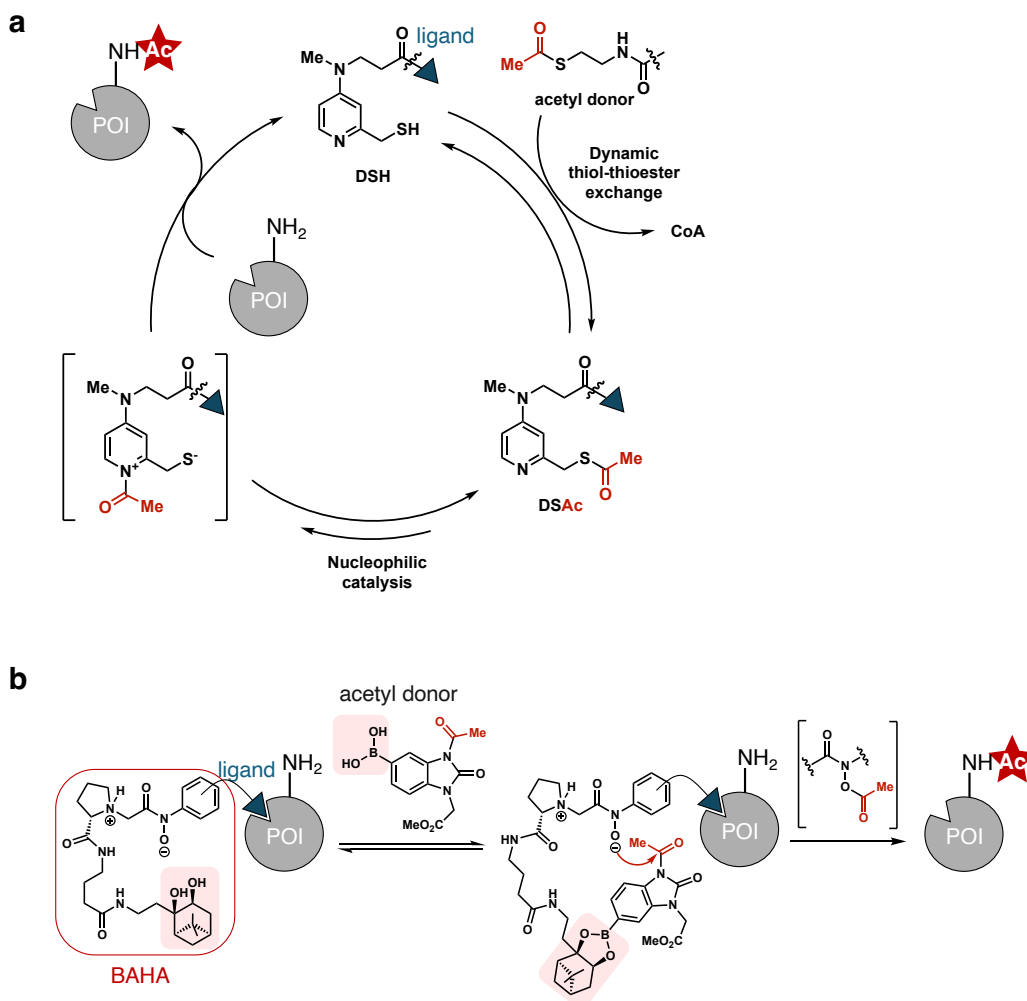
Extended Data Fig. 1: The structures and reaction mechanisms of catalytically active sites (CASs).

a, The structure of and a plausible reaction mechanism for thiol-tethered 4-dimethylaminopyridine (DSH) catalyst. **b**, The structure of and a plausible reaction mechanism for boronate-assisted hydroxamic acid (BAHA) catalyst.
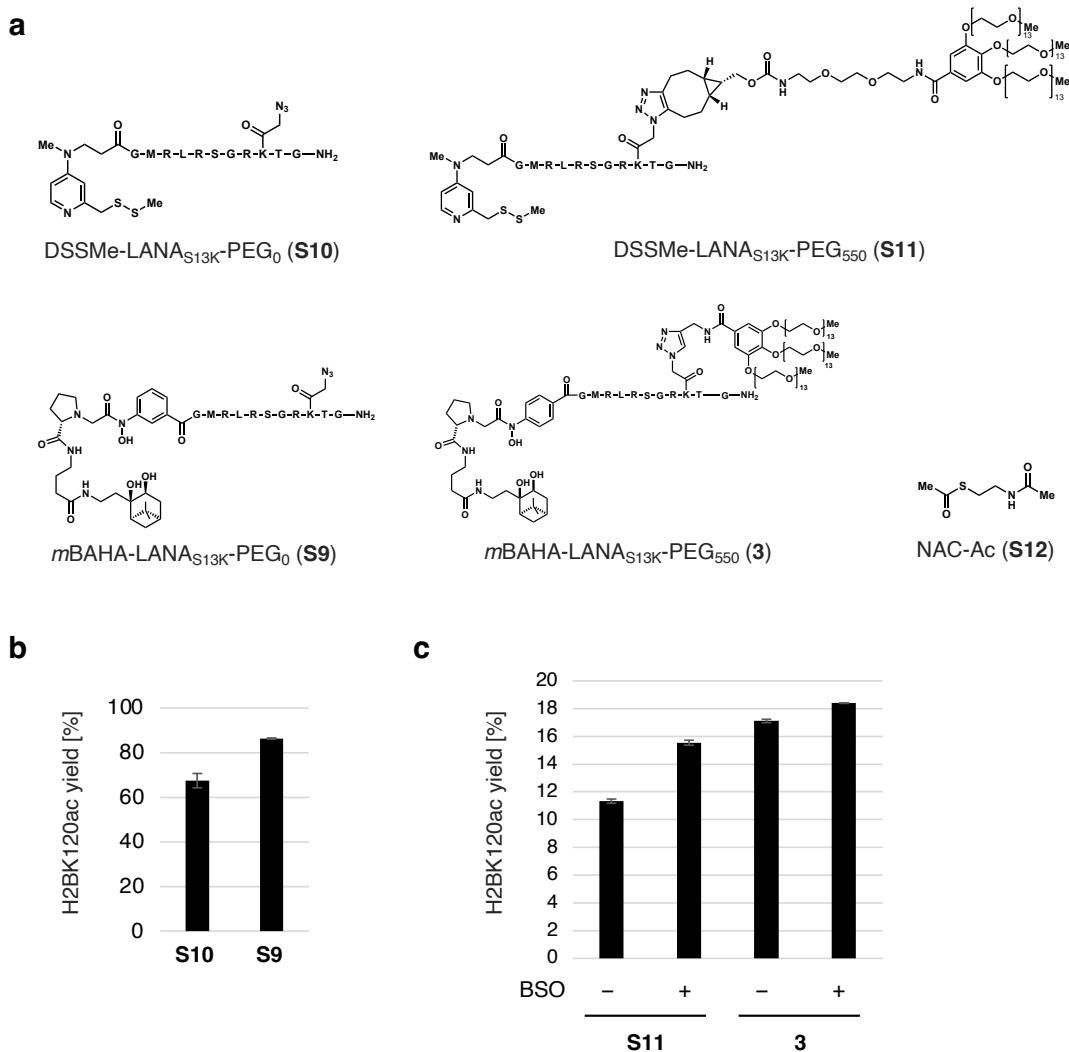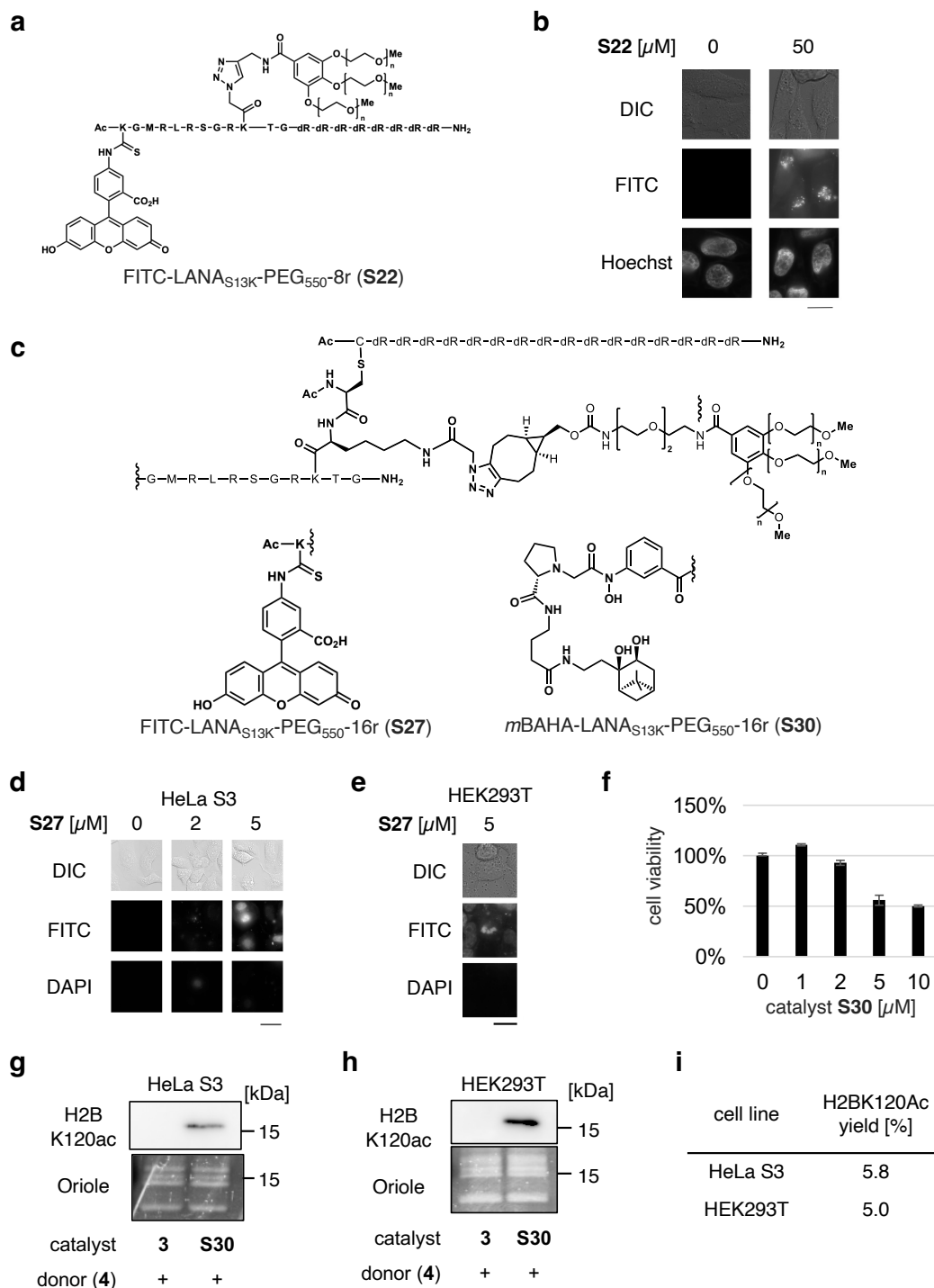
Extended Data Fig. 2: Catalyst structure optimization at the CAS motif.
a, Chemical structures of catalysts (**S10**, **S11**, **S9**, **3**) and an acetyl donor **S12**. **b**, LC-MS/MS analysis for H2BK120ac levels of recombinant nucleosomes treated with **S10** (2 μM) and NAC-Ac **S12** (10 mM) or **S9** (2 μM) and an acetyl donor **4** (0.1 mM) for 5 hours. Error bars represent the data range of two independent experiments. **c**, LC-MS/MS analysis for H2BK120ac levels in HeLa S3 cells. To cells pretreated with BSO (100 μM), **S11** (0.5 mM) and NAC-Ac **S12** (30 mM) or **3** (0.5 mM) and an acetyl donor **4** (0.4 mM) were introduced by a bead-loading method. Then cells were treated with NAC-Ac **S12** (30 mM) or acetyl donor **4** (0.4 mM) for 5 hours. The acetylation yield was calculated as the ratio of acetylated lysine to (acetylated lysine + unmodified lysine) detected by LC-MS/MS. Error bars represent the data range of two independent experiments.

27

Extended Data Fig. 3: Optimization of LANA and PEG motifs.
a, Chemical structures of catalysts **S13**-**S18**. **b**, LC-MS/MS analysis for H2BK120ac levels of recombinant nucleosomes treated with catalyst (2 µM) and NAC-Ac **S12** (10 mM) for 5 hours. Error bars represent the data range of two independent experiments. **c**, Chemical structures of catalysts **S19**-**S20**. **d**, LC-MS/MS analysis for H2BK120ac levels of recombinant nucleosomes treated with catalyst (2 µM) and NAC-Ac **S12** (10 mM) for 5 hours. The acetylation yield was calculated as the ratio of acetylated lysine to (acetylated lysine + unmodified lysine) detected by LC-MS/MS. Error bars represent the data range of two independent experiments.

a

FITC-LANA$_{S13K}$-PEG$_{550}$-8r (**S22**)

b

S22 [μM]	0	50
DIC		
FITC		
Hoechst		

c

FITC-LANA$_{S13K}$-PEG$_{550}$-16r (**S27**) mBAHA-LANA$_{S13K}$-PEG$_{550}$-16r (**S30**)

d

HeLa S3

S27 [μM]	0	2	5
DIC			
FITC			
DAPI			

e

HEK293T

S27 [μM]	5
DIC	
FITC	
DAPI	

f

cell viability vs catalyst **S30** [μM]

g

HeLa S3

		[kDa]
H2B K120ac		— 15
Oriole		— 15
catalyst	**3** **S30**	
donor (**4**)	+ +	

h

HEK293T

		[kDa]
H2B K120ac		— 15
Oriole		— 15
catalyst	**3** **S30**	
donor (**4**)	+ +	

i

cell line	H2BK120Ac yield [%]
HeLa S3	5.8
HEK293T	5.0

Extended Data Fig. 4: Conjugation of oligo-arginine as CPP.
a, Chemical structure of compound **S22**. **b**, Representative microscopic images of FITC-LANA$_{S13K}$-PEG$_{550}$-8r **S22** in HeLa S3 cells. Cells were treated with **S22** (50 µM) for 60 min. DNA was stained with Hoechst 33342 to visualize chromatin distribution. Scale bar, 20 µm. **c**, Chemical structure of compounds **S27** and **S30**.
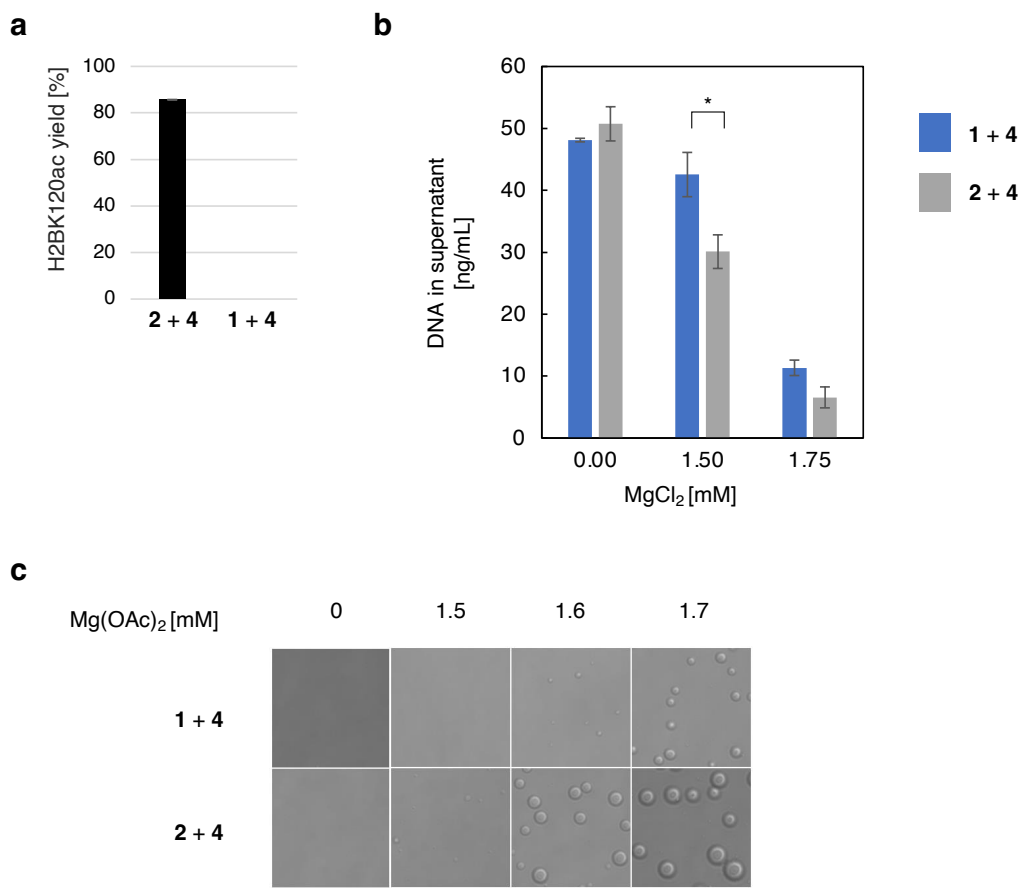
29

d-e, Representative microscopic images of FITC-LANA$_{S13K}$-PEG$_{550}$-16r **S27** in the indicated cell lines. HeLa S3 cells in **d** or THP-1 cell in **e** was treated with **S27** for 60 min. Scale bar, 30 µm in **d**, 10 µm in **e**. **f**, Cytotoxicity of catalyst **S30** (1 hour treatment) in HeLa S3 cells. Error bars represent the data range of two independent experiments. **g-h**, Immunoblot showing H2BK120ac levels in cells (**g**: HeLa S3, **h**: HEK293T) treated with *m*BAHA-LANA$_{S13K}$-PEG$_{550}$-16r **S30** (5 µM) or BAHA-LANA-PEG **3** for 1 hour and then acetyl donor **4** (0.4 mM) for 3 hours. **i**, LC-MS/MS quantification of histone acetylation. The acetylation yield was calculated as the ratio of acetylated lysine to (acetylated lysine + unmodified lysine) detected by LC-MS/MS. LC-MS/MS analysis for H2BK120ac levels in cells treated with *m*BAHA-LANA$_{S13K}$-PEG$_{550}$-16r **S30** (5 µM) for 1 hour and then acetyl donor **4** (0.4 mM) for 3 hours.
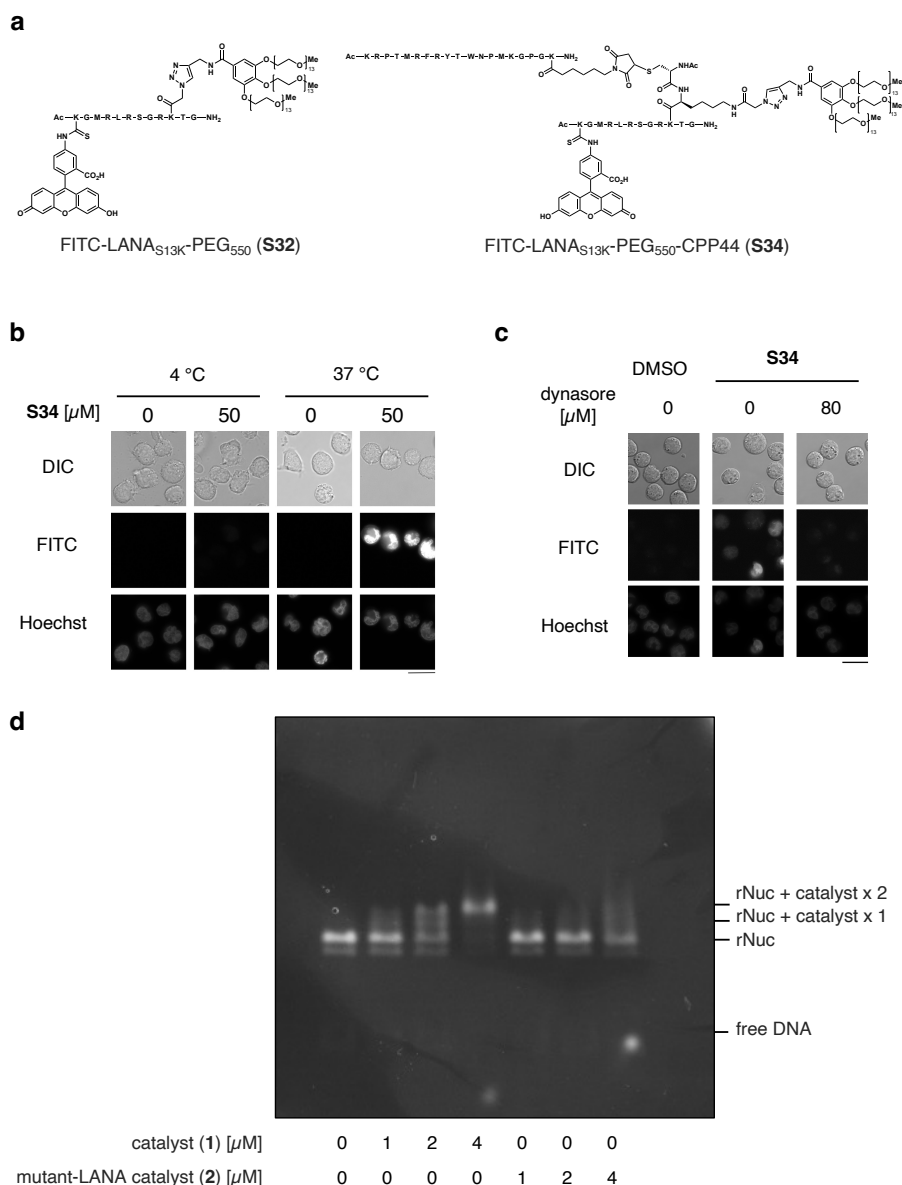
Extended Data Fig. 5: Characterization of CPP44-tethered compounds.
a, Structures of compounds **S32** and **S34**. **b-c**, Representative microscopic images of FITC-LANA$_{S13K}$-PEG$_{550}$-CPP44 **S34** in THP-1 cells. THP-1 cells were treated with **S34** (50 µM in **b**, 10 µM in **c**) for 60 min. Dynasore is the cell-permeable dynamin inhibitor. DNA was stained with Hoechst 33342 to visualize chromatin distribution. Scale bar, 20 µm. **d**, Electrophoretic mobility shift assay of recombinant nucleosomes (1 µM) incubated with BAHA-LANA-PEG-CPP44 **1** or BAHA-mutLANA-PEG-CPP44 **2**. Recombinant nucleosomes were visualized by ethidium bromide staining. Nucleosome-binding ability of BAHA-mutLANA-PEG-CPP44 **2** was significantly lower than that of BAHA-LANA-PEG-CPP44 **1**.

31

a

H2BK120ac yield [%]

100
80
60
40
20
0

Mg(OAc)₂

Catalyst/Donor

+/+

mut/+

2 + 4   **1 + 4**

350 nM 12-mer rNuc (as Nuc), 25℃, 1 h
25 mM Tris-OAc(7.5), 0.1 mM EDTA, 5% Glycerol, 5mM DTT, 0.1 mg/mL BSA
...ug/mL Glucose Oxidase, 175 ng/mL Catalase, 2 mM Glucose

b

Salt concentration [mM]

0   1.30   1.40   1.50   1.60   1.70

60
50

*

1.75

10 um

1 + 4

2 + 4

Mg(OAc)₂   0

Catalyst/Donor

+/+

mut/+

350 nM 12-mer rNuc (a...
25 mM Tris-OAc(7.5), 0...
1 ug/mL Glucose Oxida...

1.70

10 um

1.70

10 um

c

Mg(OAc)₂ [mM]   0   1.5   1.6   1.7

1 + 4

2 + 4

250
200
150
100
50
0

Purified rNuc conc [ng/uL]

826

(+/+)   (+/...

826

250
200
150
100
50
0

Purified rNuc conc [ng/uL]

(+/+)   (+/mut)

827

250
200
150
100
50
0

Purified rNuc conc [ng/uL]

(+/+)   (+/mut)

Extended Data Fig. 6: Biochemical characterization of acetylated 12-mer nucleosome array.

a, LC-MS/MS analysis for H2BK120ac levels of recombinant 12-mer nucleosomes treated with catalyst **1** or **2** (2 μM) and acetyl donor **4** (0.1 mM) for 2 hours. The acetylation yield was calculated as the ratio of acetylated lysine to (acetylated lysine + unmodified lysine) detected by LC-MS/MS. Error bars represent the data range of two independent experiments. **b,** Recombinant 12-mer nucleosome array was treated with catalyst **1** or **2** (2 μM) and acetyl donor **4** (0.1 mM) for 2 hours. Then, the nucleosome arrays were analyzed in Mg²⁺-promoted sedimentation assay. Error bar represents the standard error of four independent experiments. *$P < 0.05$ in Student's *t*-test. **c**, Recombinant 12-mer nucleosome array was treated with catalyst **1** or **2** (2 μM) and acetyl donor **4** (0.1 mM) for 2 hours. Then, the nucleosome arrays were analyzed in phase separation assay. Scale bar, 10 μm.

32
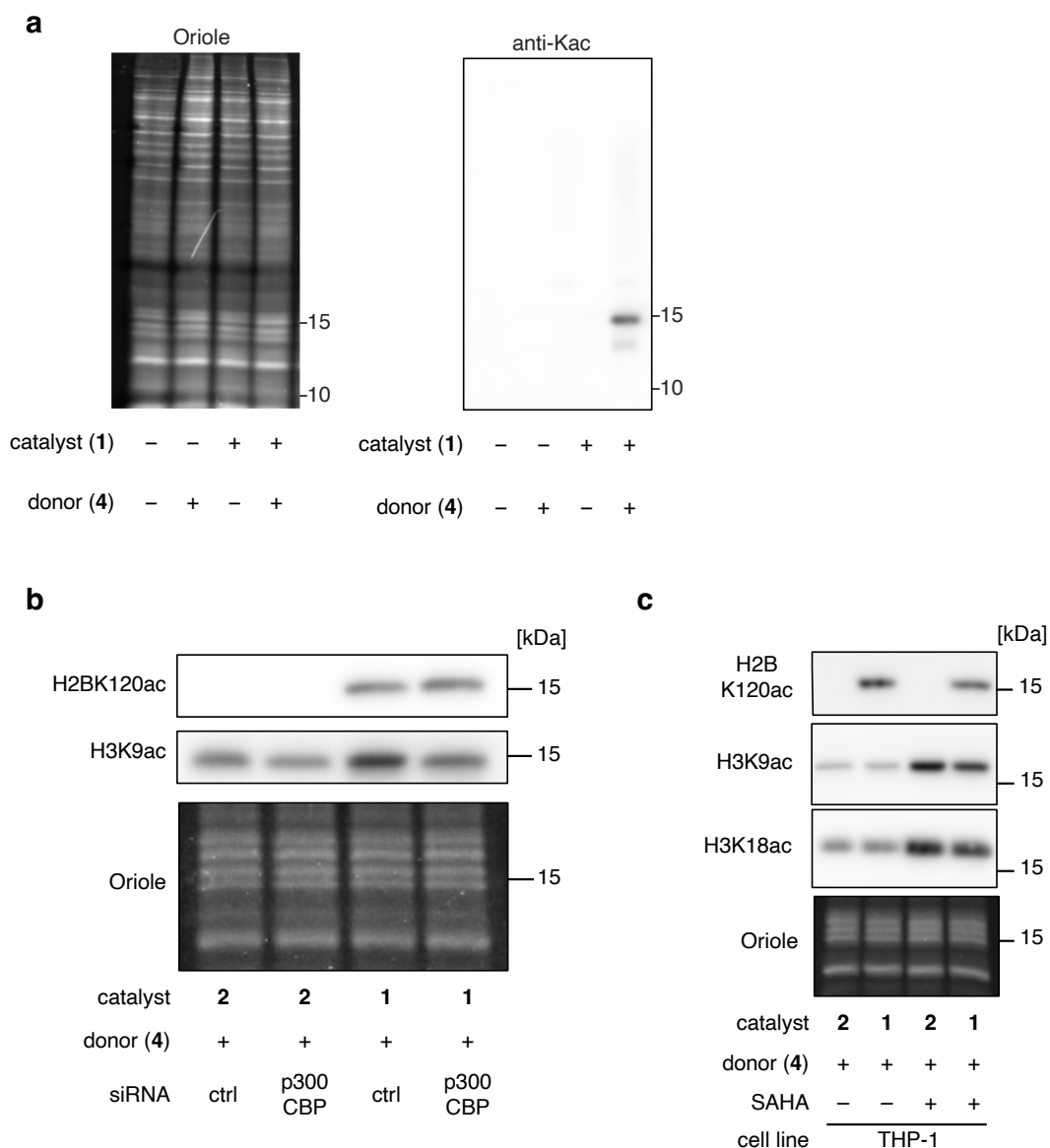
Extended Data Fig. 7: Protein-selectivity and HAT- or HDAC-dependency of catalytic histone acetylation.

a, Immunoblot showing H2BK120ac levels in whole cell extract of THP-1 cells treated with catalyst **1** (10 μM) and acetyl donor **4** (1 mM) for 2 hours. **b**, Immunoblot showing H2BK120ac and H3K9ac levels in THP-1 cells transfected with control or p300- and CBP-specific siRNA, followed by treatment with catalyst **1** or **2** (10 μM) and acetyl donor **4** (1 mM) for 2 hours. **c,** Immunoblot showing histone modification levels in THP-1 cells treated with catalyst **1** or **2** (10 μM) and acetyl donor **4** (1 mM) in the presence or absence of SAHA (2 μM) for 2 hours.
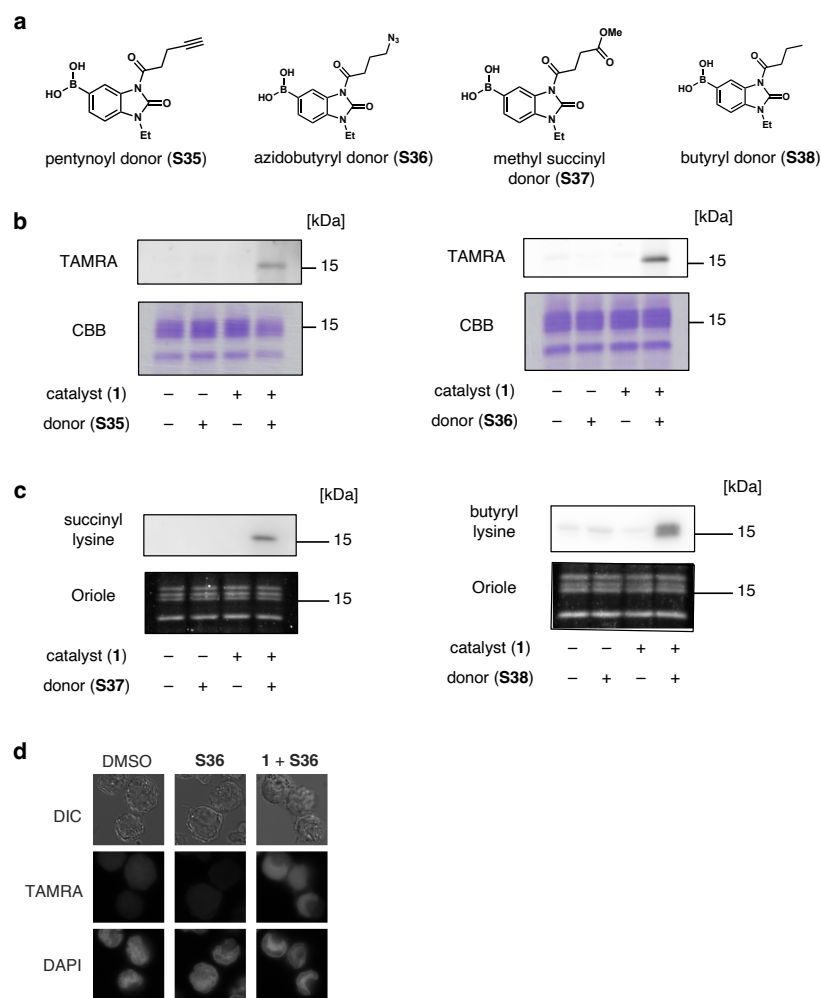
Extended Data Fig. 8: Catalyst histone acylation in THP-1 cells.

a, Structures of acyl donors **S35-S38**. **b**, THP-1 cells were treated with catalyst **1** (10 µM) and acyl donor **S35** or **S36** (0.1 mM) for 1 hour. Then histones were extracted by acid extraction. To detect acylation containing alkyne or azide, acylated lysines were labeled with TAMRA-azide or TAMRA-alkyne, respectively, by Cu(I)-catalyzed azide-alkyne cycloaddition reaction. The fluorescence detection is shown (TAMRA). Proteins were visualized by CBB staining. **c**, THP-1 cells were treated with catalyst **1** (10 µM) and acyl donor **S37** or **S38** (0.1 mM) for 1 hour. Then histones were extracted by acid extraction and analyzed by immunoblotting with anti-succinyl lysine or anti-butyryl lysine antibody. **d**, Representative microscopic images of THP-1 cells treated with catalyst and acyl donor. Cells were treated with catalyst **1** (10 µM) and azidobutyryl donor **S38** (0.1 mM) for 60 min, followed by fixation and click reaction with TAMRA-alkyne. Scale bar, 10 µm.

34

a

b

c
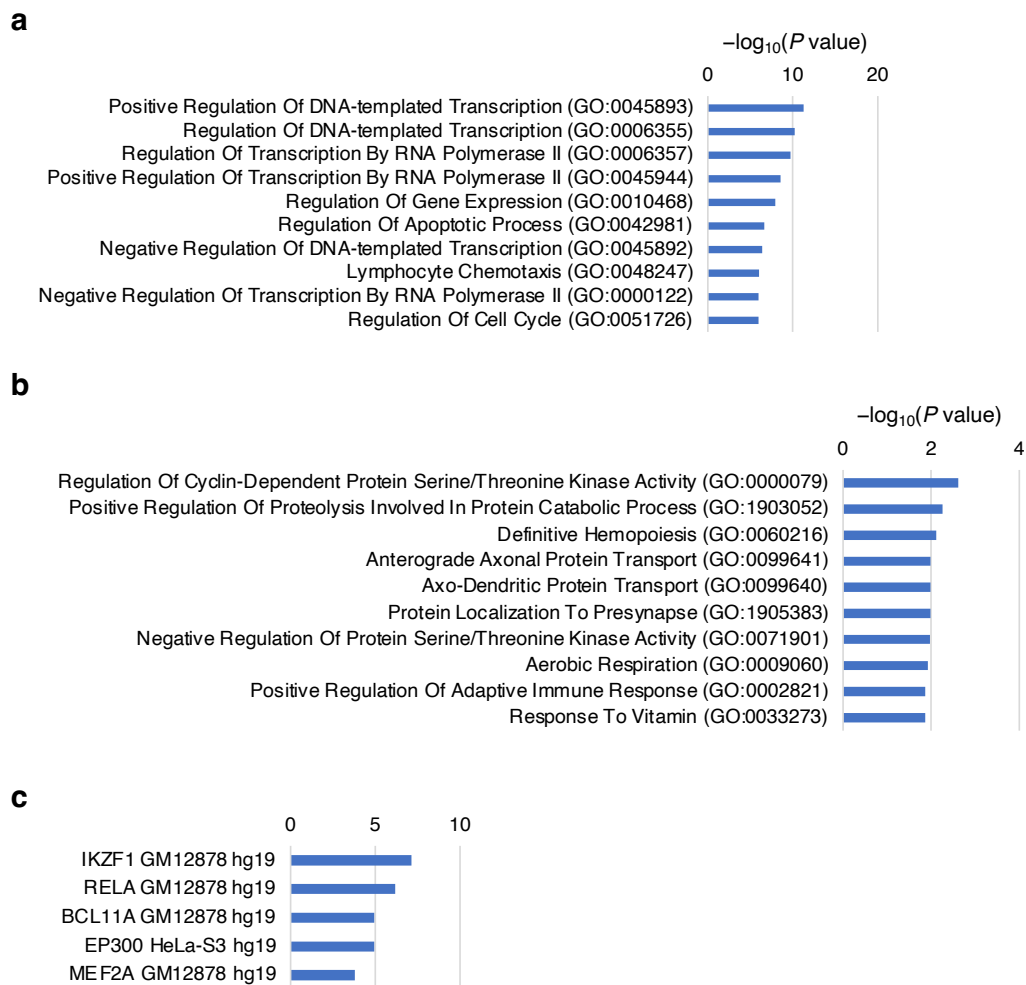
Extended Data Fig. 9: Enrichment analysis of RNA-seq after catalytic histone acetylation in THP-1 cells.

a, Top-10 enriched clusters of biological processes from GO-term enrichment analysis of 634 upregulated genes by acetylation for 4 hours ($P < 0.05$, $\log_2 FC > 1$). **b**, Top-10 enriched clusters of biological processes from GO-term enrichment analysis of 466 downregulated genes by acetylation for 4 hours ($P < 0.05$, $\log_2 FC < -1$). **c**, Top-5 enriched clusters of ENCODE TF ChIP-seq 2015 library from enrichment analysis of 105 downregulated genes by acetylation for 45 min ($\log_2 FC < -1$).
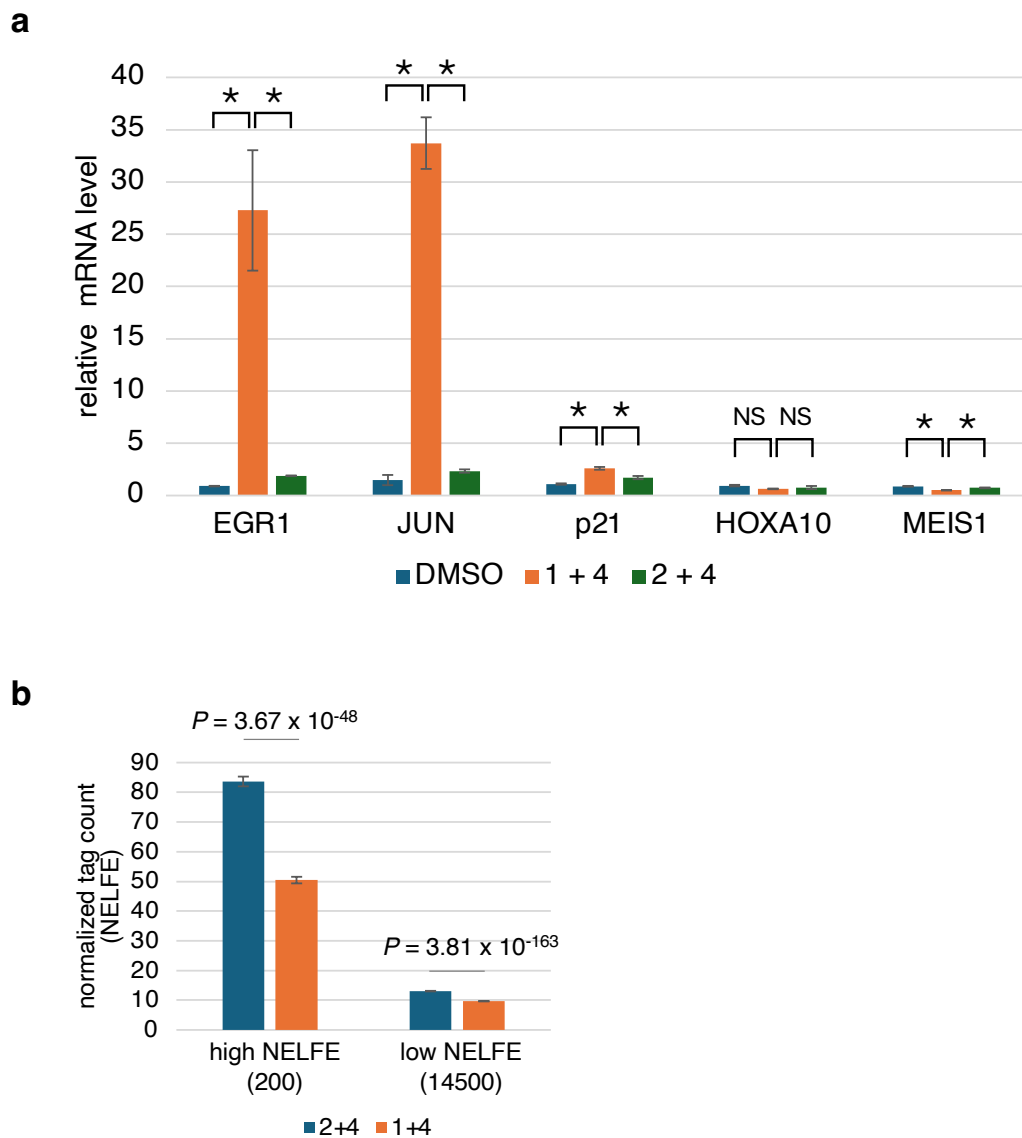
Extended Data Fig. 10: The effects of catalytic histone acetylation for transcription or chromatin localization of NELFE.

a, THP-1 cells were treated with catalyst **1** or **2** (10 µM) and acetyl donor **4** (1 mM) for 4 hours. Then, mRNAs were purified and analyzed by RT-qPCR. Error bars represent the standard deviation of three independent experiments (*$P <$ 0.05, one-way ANOVA with Tukey's post hoc test, NS: not significant). **b**, Comparison of the change of normalized tag count of NELFE ChIP-seq after catalytic histone acetylation for high NELFE genes (n = 200) and low NELFE genes (n = 14,500). The P-value was calculated by Student's t-test. Data are shown as mean ± SEM.

36

Material and Methods

<u>Statistics and reproducibility</u>

Statistical analyses were performed using Microsoft Excel (version 16.83) or R (version 4.3.2). *P* values were determined by Student's *t*-tests, one-way ANOVA with Tukey's post hoc tests, log-rank tests, or Fisher's exact tests as appropriate and as listed in the figure legends. The statistical significances of differences are specified throughout the figures and legends. For in-test-tube experiments, each experiment was performed in duplicate, and only small variations between individual results were observed in all of the experiments. For in-cell experiments, each experiment was performed in n = 3-4, as indicated in the figure legends.

<u>Cell culture</u>

THP-1 (JCRB0112, purchased from JCRB Cell Bank), MOLM-13 (JCRB1810, purchased from JCRB Cell Bank), MV-4-11 (CRL-9591, purchased from ATCC), Kasumi-1 (JCRB1003, purchased from JCRB Cell Bank) and K562 (gifted from Kitagawa Lab) cells were grown in RPMI medium 1640 (Gibco, 11875) with 10% fetal bovine serum (FBS; Gibco), 100 U/mL penicillin and 100 μg/mL streptomycin (Gibco) at 37 °C in an atmosphere of 5% CO_2. HeLa S3 (gifted from Gotoh Lab) and HEK293T (gifted from Hirota Lab) cells were grown in Dulbecco's modified Eagle medium (DMEM; Gibco, 12430) with 10% fetal bovine serum (FBS; Gibco), 1x GlutaMAX (Gibco) 100 U/mL penicillin and 100 μg/mL streptomycin (Gibco) at 37 °C in an atmosphere of 5% CO_2. If necessary, 2 μM SAHA (Sigma, SML0061) was supplemented to the growth medium. Cryopreserved Peripheral Blood Mononuclear Cells (PBMC) were purchased from HemaCare (PB009C-1) and used for experiments soon after thawing.

<u>Antibodies</u>

Rabbit polyclonal antibodies against H3K9ac (Merck, 07–352), H3K18ac (abcam, ab1191) and NELFE (proteintech, 10705-1-AP, for ChIP-seq), a rabbit monoclonal antibody against H2B ubiquitination (Cell signaling technology, 5546S), mouse monoclonal antibodies against H2BK120ac[20], NELFE (Santa Cruz Biotechnology, sc-377052, for western blotting), unphosphorylated RNA Pol II[46] were used for western blotting and ChIP-seq.

<u>Fluorescent microscopy for living cells using CPP44-tethered compounds</u>

To observe the subcellular distribution of fluorescein isothiocyanate (FITC)-labeled compounds in living cells, cells were washed twice with PBS and treated with the FITC-labeled compounds in serum-free growth medium for 60 min. at 4 °C or 37 °C. Then, the cells were washed twice with PBS, and then imaged by fluorescent microscopy (DMi8; Leica). For mechanism study of catalyst internalization, the cells were pre-treated with 80 µM dynasore for 60 min.

Cell viability assay

After catalyst-promoted histone acetylation, the cells were washed once with PBS, resuspended in fresh growth medium and mixed with CellTiter-Glo® 2.0 Reagent (Promega). After 10 min. incubation at r.t., the luminescent signal was measured by GloMax® Discover Microplate Reader (Promega). The cell viability was calculated by dividing the luminescent signal of the cells treated with compounds by the luminescent signal of the cells treated with DMSO.

Catalyst-promoted acetylation of recombinant mononucleosomes

Recombinant nucleosomes were prepared as described previously[47]. Recombinant nucleosomes (0.37 µM for DNA/histone octamer concentration) were mixed with catalyst, acetyl donor, TCEP (0 mM in Fig. 3 and 0.1 mM in Extended Data Fig. 2-3) in 20 mM Tris-HCl (pH 7.5) and incubated for indicated time at 37 °C.

Western blotting analysis

After catalyst-promoted histone acetylation, the cells were washed once with PBS and lysed in pre-chilled CRB buffer (50 mM Tris-HCl (pH 7.5), 300 mM NaCl, 0.3% Triton X-100) supplemented with 2 mM $MgCl_2$, 25 mU/µL Benzonase, protease inhibitor cocktail (Sigma), and 1 mM PMSF on ice for 30 min. After centrifugation (15,000 rpm for 5 min. at 4 °C), the supernatants were separated by sodium dodecyl sulfate-polyacrylamide gel electrophoresis (SDS-PAGE) followed by oriole (Bio-Rad) or CBB (45 g citric acid monohydrate (Sigma), 15 g β-Cyclodextrin (Wako), 0.24 g CBB R-250 (Wako) in 3 L Milli-Q water) staining. After equalizing the protein concentration, the proteins were analyzed by western blotting.

Catalyst-promoted histone acetylation in living cells

Cells were washed twice with PBS and treated with catalyst and acetyl donor. For

38

2-hour or 45-min. reaction, the cells were treated with catalyst and acetyl donor in serum-free growth medium for 2 hours or 45 min. at 37 °C. For 4-hour reaction, firstly the cells were treated with catalyst and acetyl donor in serum-free growth medium for 2 hours at 37 °C. Then, the cells were incubated in serum-containing growth medium for 1 hour at 37 °C, followed by double PBS wash and another 2-hour reaction by adding new catalyst and acetyl donor.

LC-MS/MS analysis and quantification of the stoichiometry of acetylation

For recombinant nucleosomes, the acetylated nucleosomes and were precipitated by trichloroacetic acid (16.6%). After DNA was digested by DNase I (Takara) for 30 min. at 37 °C, the samples were mixed with acetone (74%). After overnight incubation at −30 °C, the proteins were collected by centrifugation, air dried and dissolved in Milli-Q water. For acid extracted histones from cells, the histones were dissolved in Milli-Q water and incubated for 10 min. at 25 °C.

To the solution of histones, 50 mM aqueous ammonium bicarbonate (NH_4HCO_3 aq.) and 25% propionic anhydride solution (methanol/propionic anhydride, 3:1 (vol/vol)) were added, and pH was adjusted to 8 by adding ammonia solution. After 30-min. incubation at 25 °C, the solvents were removed by Speed-Vac evaporator. The samples were resuspended in 50 mM NH_4HCO_3 aq. with 0.1% ProteaseMAX (Promega) and digested with 10 ng/µL Trypsin Gold (Promega), 10 ng/µL Glu-C (Promega) in 50 mM NH_4HCO_3 aq. with 0.02% ProteaseMAX at 37 °C for 3 hours or overnight. Then, 5% aqueous formic acid (vol/vol) was added, and the solvents were removed by Speed-Vac evaporator to obtain dried digested samples, which were dissolved in 0.1% aqueous formic acid (vol/vol). After centrifugation (15,000 rpm, 5 min.), the supernatant was used for LC-MS/MS analysis (Triple TOF 6600 (AB Sciex) equipped with M5 micro LC (AB Sciex)) as previously reported[20]. Data analysis was carried out using PeakView software (AB Sciex), and the average values were obtained from duplicated measurements. The stoichiometry of acetylated lysines was calculated as a percentage of the total peak area of the extracted ion chromatogram for acetylated peptides in the sum of those for acetylated peptides and propionylated peptides.

RNA-seq

After catalyst-promoted histone acetylation, RNA was extracted from the cells with NucleoSpin® RNA (Takara). TruSeq Stranded mRNA Sample Prep Kit

39

(Illumina) was used to prepare the library for RNA-seq. Deep sequencing was performed on Illumina NovaSeq platform according to the manufacturer's protocol.

ChIP-seq

After catalyst-promoted histone acetylation, 1.0×10^7 cells were fixed with 1% paraformaldehyde (freshly prepared from powder, filtered before use) in 1 mL PBS for 10 min. at 25 °C, which was quenched by addition of 80 µL 1.25 M glycine in PBS. Then the cells were washed twice with ice-cold PBS and suspended in 156 µL SDS lysis buffer (50 mM Tris-HCl (pH 8.0), 1% SDS, 10 mM EDTA, protease inhibitor cocktail). After 10 min. incubation on ice, the cells were sonicated with BioRaptor® II (BM Equipment Co). The supernatants were diluted 10-fold with ChIP dilution buffer (16.7 mM Tris-HCl (pH 8.0), 0.01% SDS, 1.1% TritonX-100, 1.2 mM EDTA, 167 mM NaCl) and the DNA concentrations were adjusted by measurement with Nanodrop® lite (Thermo). If needed, spike-in chromatin (active motif) was added. Then, 1500 µL of extract was added to Dynabeads® Protein G (40 µL, Veritas), which was pre-incubated with antibodies (4 µg for anti-H2BK120ac or NELFE antibodies and 10 µg for anti-RNA Pol II antibodies) for ChIP and 2 µg spike-in antibodies (active motif) for 20 hours at 4 °C with rotating. Then the mixture was incubated for 48 hours at 4 °C with rotating. After incubation, the beads were washed with LS buffer (20 mM Tris-HCl (pH 8.0), 150 mM NaCl, 0.1% SDS, 1% Triton X-100, 2 mM EDTA), HS buffer (20 mM Tris-HCl (pH 8.0), 500 mM NaCl, 0.1% SDS, 1% Triton X-100, 2 mM EDTA), LiCl buffer (10 mM Tris-HCl (pH 8.0), 0.25 M LiCl, 1% NP-40, 1% sodium deoxycholate, 1 mM EDTA) and TE buffer (10 mM Tris-HCl (pH 8.0), 1 mM EDTA), followed by extraction with elution buffer (100 mM NaHCO3, 1% SDS, 10 mM DTT). The supernatant was incubated with 200 mM NaCl for 16 hours at 65 °C, and treated with proteinase K for 1 hour at 45 °C. DNA was purified from the supernatant of ChIP samples by PCR Clean-Up Mini Kit (Favorgen). ChIP libraries were constructed using the KAPA Hyper Prep Kit (Kapa Biosystems, Inc., Wilmington, MA, USA) according to the manufacturer's instructions, quantified using Bioanalyzer (Aglient), and sequenced on the Illumina NovaSeq according to the manufacturer's protocol.

RNA-seq and ChIP-seq analysis

Sequenced reads in ChIP-seq experiment were mapped to UCSC human genome (hg19) using bowtie. Duplicated reads were removed with Picard tools.

Peak count was performed by using HOMER software (http://homer.salk.edu/homer/index.html). Metagene profiles were produced with the use of deepTools (https://deeptools.readthedocs.io/en/develop/). Enrichment and Gene Ontology (GO) analysis was performed by using Enrichr (https://maayanlab.cloud/Enrichr/). For analysis for MLL-target genes, the gene set named "Human Gene Set: KUMAR_TARGETS_OF_MLL_AF9_FUSION" was used.

Flow cytometric analysis of cell cycle

After catalyst-promoted histone acetylation, the cells were washed once with PBS and resuspended in pre-chilled 70% ethanol. After 3 hours of fixation at −30 °C, the cells were washed once with PBS and mixed with Muse cell cycle reagent (Luminex). After 30 min. incubation at 25 °C, the cells were analyzed by Muse cell analyzer (Merck).

Flow cytometric analysis of apoptosis

After catalyst-promoted histone acetylation, the cells were washed once with PBS, resuspended in fresh growth medium and mixed with Muse annexin V & dead cell reagent (Luminex). After 20 min. incubation at 25 °C, the cells were analyzed by Muse cell analyzer (Merck).

Cell proliferation analysis

After catalyst-promoted histone acetylation, the cells were washed once with PBS and resuspended in fresh growth medium. Then, the cells were plated in 96-well plates at a density of 2×10^5 cells/mL in a final volume of 200 μL. The number of tripan-blue negative living cells were counted with TC20 automated cell counter (Bio-Rad), and the cells were replated at equal cell numbers in fresh growth medium every 2 days.

Mice experiments

Animal experiments were performed in accordance with the institutional guidelines for the use of laboratory animals and approved by the Review Board for Animal Experiments of the University of Tokyo (approval ID, PA18-42). NOD.Cg-Prkdcscid Il2rgtm1Sug/ShiJic (NOG) were purchased from In-Vivo Science Inc. The AkaBLI system, composed of AkaLumine-HCl and Akaluc, provides a light source of sufficient strength to penetrate body walls, even in deep

41

tissue areas . Akaluc was introduced into MOLM-13 cells using the CS-CDF-UbC-mScarlet-P2A-Akaluc-PRE lentivirus to confirm tumor burden in mice[48]. After catalyst-promoted histone acetylation, the cells were washed once with PBS and resuspended in PBS. Then, the cells (3×10^6 cells) were injected to NOG mice. To monitor the tumor burden, one hundred microliters of 5 mM AkaLumine-HCl (Wako) was injected intraperitoneally into mice immediately before image analysis, and mice under isoflurane anesthesia were imaged within 5–10 min after injection. The signal intensity was measured using an IVIS (Perkin Elmer).

Acknowledgments

Author contributions

S.A.K. and M.K. conceived and designed the project. Y.Y., S.T., and Y.A. performed the experiments and synthesized all chemical compounds. K.Y. supervised synthesis of compounds. A.O. and A.K performed RNA-seq and ChIP-seq. Y.R.K. purified 12-mer nucleosome array and performed experiments. T.K. and H.Ku. purified recombinant mononucleosomes. S.K. and A. I. performed mouse experiments. Y.Y., S.A.K., and M.K. wrote the manuscript with

contributions from all other authors.

Competing interests

Authors declare that they have no competing interests.

Data and materials availability

Next-generation sequencing data generated during this study have been deposited in Gene Expression Omnibus (GSE259436 and GSE259437). All other data are available in the manuscript or the supplementary material.

Supplementary Information is available for this paper.

Correspondence and requests for materials should be addressed to Motomu Kanai (kanai@mol.f.u-tokyo.ac.jp).

43